

Bayesian nonstationary Gaussian process modeling: the **BayesNSGP** package for R

Mark D. Risser^a and Daniel Turek^b

^a Lawrence Berkeley National Laboratory

^b Williams College

Abstract

In spite of the diverse literature on nonstationary Gaussian process modeling, the software for implementing convolution-based methods is extremely limited, particularly for fully Bayesian analysis. To address this gap, here we present the **BayesNSGP** software package for R that enables off-the-shelf functionality for fully Bayesian, nonstationary Gaussian process modeling. Our approach to nonstationary modeling involves a closed-form, convolution-based covariance function with spatially-varying parameters; these parameter processes can be specified either deterministically (using covariates or basis functions) or stochastically (using approximate Gaussian processes). Stationary Gaussian processes are a special case of our methodology, and we furthermore implement approximate Gaussian process inference to account for very large spatial data sets. Bayesian inference is carried out using Markov chain Monte Carlo methods via the **nimble** package, which enables sampling of the highly correlated parameter spaces common to Gaussian process models (e.g., using adaptive block Metropolis-Hastings sampling). Posterior prediction for the Gaussian process at unobserved locations is also implemented as a straightforward post-processing step. As a demonstration, we use the package to analyze three data sets: first, the relatively small precipitation data set from Colorado that is used as a test case for related nonstationary methodology; second, a larger precipitation data set from a set of in situ measurements over the contiguous United States (with $N \approx 1500$ weather stations); and finally, a very large data set of return values for Boreal winter mean temperature at the surface derived from a general circulation model (with $N \approx 50,000$ grid cells).

Keywords: Spatial statistics, spatially-varying parameters, process convolution, nearest neighbor Gaussian process, sparse general Vecchia, large data, **nimble**

1 Introduction

Gaussian processes (GPs) are an extremely popular tool in modern statistical modeling, with broad application in spatial and environmental statistics as well as machine learning and emulation of complex mathematical models. On the practical side, GPs are popular as a form of nonparametric or nonlinear regression, as they characterize a nonlinear relationship

between a set of inputs and an output. On the technical side, GPs are a default choice for modeling point-referenced, continuously-indexed processes (spatial or otherwise) because all finite-dimensional distributions are known to be Gaussian and because the GP is completely specified by a characterization of its first- and second-order properties. Furthermore, the second-order properties can be specified via widely used classes of valid covariance functions.

Among the broad literature on covariance function modeling, many traditional approaches are based on assumptions of isotropy or stationarity, which specify that the covariance between the process of interest at two different locations (or inputs) is a function of only the separation distance or separation vector, respectively. Assumptions of stationarity are made primarily for convenience, as it is rarely a realistic assumption for real world data sets. As a result, the literature contains a wide variety of nonstationary covariance function models for Gaussian process models (e.g., [Sampson and Guttorp, 1992](#); [Higdon, 1998](#); [Damian et al., 2001](#); [Fuentes, 2001](#); [Schmidt and O’Hagan, 2003](#); [Paciorek and Schervish, 2006](#); [Lindgren et al., 2011](#)), which allow the spatial dependence structure to vary over the domain of interest. Unfortunately, while these approaches more appropriately characterize the covariance structure of a process, most are also highly complex and require intricate algorithms for model fitting. A second thread in the literature addresses this problem by characterizing nonstationarity in terms of covariates (e.g., [Calder, 2008](#); [Schmidt et al., 2011](#); [Reich et al., 2011](#); [Vianna Neto et al., 2014](#); [Risser and Calder, 2015](#)), which aids both implementation and interpretation of the resulting nonstationarity. We refer the interested reader to [Risser \(2016\)](#) for further detail on these various methodologies.

In spite of the diverse literature on nonstationary GP modeling (covariate-based or otherwise), there are very few methods that offer software—particularly in a Bayesian setting—making it difficult for a general practitioner to use most of these approaches. The **fields** package ([Nychka et al., 2014](#)) and **convoSPAT** package ([Risser and Calder, 2017](#)) provide software for Frequentist inference for nonstationary spatial processes, while packages like **INLA** ([Lindgren et al., 2011](#); [Ingebrigtsen et al., 2014](#); [Fuglstad et al., 2015](#); [Lindgren and Rue, 2015](#)), **spBayes** ([Finley et al., 2007](#)), and **tgp** ([Gramacy, 2007](#)) provide software for fully Bayesian analysis. Note, however, that while the predictive process method of [Banerjee et al. \(2008\)](#) implemented in **spBayes** is technically nonstationary, the model has only trivial differences from a stationary covariance function. While these are a flexible set of tools, none of these approaches implement fully Bayesian analysis of convolution-based or spatially-varying parameter methods (e.g., [Higdon et al., 1999](#); [Paciorek and Schervish, 2006](#)), which both flexibly model nonstationary processes (by allowing the parameters of the covariance function to vary over space) and also yield interpretable summaries of how and why a process exhibits nonstationarity (see [Risser and Calder, 2015, 2017](#)). Furthermore, other than **INLA**, none of the available nonstationary software includes modern advances in approximate Gaussian process modeling that enable inference for very large data sets (see [Heaton et al., 2018](#), for a summary of recent methods).

To address these shortcomings in the existing software for convolution-based GP modeling, we present the **BayesNSGP** package for R that enables off-the-shelf functionality for fully Bayesian, nonstationary Gaussian process modeling and is scalable to very large data sets. Our convolution-based approach uses a flexible nonstationary covariance function that allows spatially-varying parameters to be specified either deterministically (using covariates or basis functions) or stochastically (using approximate Gaussian processes). Stationary Gaus-

sian processes are a special case of our methodology, and we utilize the **nimble** (de Valpine et al., 2017) package to implement flexible Markov chain Monte Carlo methods for sampling the highly correlated parameter spaces common to nonstationary Gaussian process models. Posterior prediction for the Gaussian process at unobserved locations is also implemented for both full and approximate GP methods as a straightforward post-processing step.

As a final note, we mention that our package assumes a Gaussian likelihood for the data, making it inappropriate for data analyses that require non-Gaussian likelihoods (e.g., count data or highly skewed data). Of course, our methodology could be applied in a hierarchical model that assigns a Gaussian process to a latent process in the statistical model (e.g., the log intensity function for Poisson data); in this case we would need to sample the latent process inside the Markov chain Monte Carlo, which is nontrivial when dealing with even moderately sized data sets. We refer the interested reader to Bradley et al. (2017) for recent developments in modeling dependent data for more general likelihoods from the natural exponential family.

The paper proceeds as follows. Section 2 outlines a canonical Bayesian nonstationary Gaussian process model as well as prediction for unobserved locations; Section 3 outlines a modeling framework for the nonstationary covariance function. Section 4 describes approximate Gaussian process inference for very large data sets and corresponding approximate posterior prediction for unobserved locations. Section 5 describes implementation in **nimble**, and Section 6 demonstrates the benefits of our approach through three examples. Section 7 concludes the paper.

2 Canonical Bayesian Gaussian process model

A general modeling framework for a univariate spatial Gaussian process can be defined as follows via a linear mixed model. Define $\{z(\mathbf{s}) : \mathbf{s} \in G\}$ to be the observed value of a spatial process over a domain $G \subset \mathcal{R}^d$, with $d \geq 1$. The mixed model can be written as

$$z(\mathbf{s}) = y(\mathbf{s}) + \varepsilon(\mathbf{s}), \quad (1)$$

where $E[z(\mathbf{s})] = y(\mathbf{s})$, $y(\cdot)$ is a spatial random effect, and $\varepsilon(\cdot)$ is a stochastic component that represents measurement error or microscale variability and is independently distributed as $N(0, \tau^2(\mathbf{s}))$ such that $\varepsilon(\cdot)$ and $y(\cdot)$ are independent. The spatial random effect is modeled as a parametric Gaussian process, denoted $y(\cdot) \sim GP(\mathbf{x}(\cdot)^\top \boldsymbol{\beta}, C_y(\cdot, \cdot; \boldsymbol{\theta}_y))$, such that $E[y(\mathbf{s})] = \mathbf{x}(\mathbf{s})^\top \boldsymbol{\beta}$ is a linear (deterministic) mean function in a set of $p-1$ covariates (with an intercept, i.e., $\mathbf{x}(\mathbf{s}) = (1, x_1(\mathbf{s}), \dots, x_{p-1}(\mathbf{s}))^\top \in \mathcal{R}^p$). The covariance function C_y is assumed known up to a vector of parameters $\boldsymbol{\theta}_y$ and describes the covariance between the process $y(\cdot)$ as

$$C_y(\mathbf{s}, \mathbf{s}'; \boldsymbol{\theta}_y) \equiv \text{Cov}(y(\mathbf{s}), y(\mathbf{s}')),$$

for all $\mathbf{s}, \mathbf{s}' \in G$. Finally, we suppose that the error variance process $\tau^2(\cdot)$ is known up to a vector of parameters $\boldsymbol{\theta}_z$.

For a fixed, finite set of N observed spatial locations $\mathcal{S}_O = \{\mathbf{s}_1, \dots, \mathbf{s}_N\} \in G$, (1) implies that the random (observed) vector $\mathbf{z}_O = [z(\mathbf{s}_1), \dots, z(\mathbf{s}_N)]^\top$ has a multivariate Gaussian distribution

$$p(\mathbf{z}_O | \mathbf{y}_O, \boldsymbol{\theta}_z) = N(\mathbf{y}_O, \boldsymbol{\Delta}(\boldsymbol{\theta}_z)), \quad (2)$$

where $\Delta(\boldsymbol{\theta}_z) = \text{diag}[\tau^2(\mathbf{s}_1), \dots, \tau^2(\mathbf{s}_N)]$. Conditional on the other parameters in the model, the process vector $\mathbf{y}_O = [y(\mathbf{s}_1), \dots, y(\mathbf{s}_N)]^\top$ is distributed as

$$p(\mathbf{y}_O | \boldsymbol{\beta}, \boldsymbol{\theta}_y) = N(\mathbf{X}_O \boldsymbol{\beta}, \boldsymbol{\Omega}(\boldsymbol{\theta}_y)), \quad (3)$$

where $\mathbf{X}_O = [\mathbf{x}(\mathbf{s}_1)^\top, \dots, \mathbf{x}(\mathbf{s}_N)^\top]^\top$ and the elements of $\boldsymbol{\Omega}(\boldsymbol{\theta}_y)$ are $\Omega_{ij} \equiv C_y(\mathbf{s}_i, \mathbf{s}_j; \boldsymbol{\theta}_y)$. Given the Gaussian distributions in (2) and (3), for certain applications it is often useful to integrate over the process $y(\cdot)$ to arrive at the marginal distribution for $z(\cdot)$, which is

$$p(\mathbf{z}_O | \boldsymbol{\beta}, \boldsymbol{\theta}) = \int p(\mathbf{z}_O | \mathbf{y}_O, \boldsymbol{\theta}_z) p(\mathbf{y}_O | \boldsymbol{\beta}, \boldsymbol{\theta}_y) d\mathbf{y}_O = N(\mathbf{X} \boldsymbol{\beta}, \Delta(\boldsymbol{\theta}_z) + \boldsymbol{\Omega}(\boldsymbol{\theta}_y)) \quad (4)$$

where $\boldsymbol{\theta} = (\boldsymbol{\theta}_z, \boldsymbol{\theta}_y)$. The covariance function for the marginalized process is

$$C_z(\mathbf{s}, \mathbf{s}'; \boldsymbol{\theta}) = C_y(\mathbf{s}, \mathbf{s}'; \boldsymbol{\theta}_y) + \tau(\mathbf{s})\tau(\mathbf{s}')I_{\{\mathbf{s}=\mathbf{s}'\}}, \quad \text{for all } \mathbf{s}, \mathbf{s}' \in G, \quad (5)$$

where $I_{\{\cdot\}}$ is an indicator function.

To complete the Bayesian specification of this model, we define prior distributions for the unknown mean and covariance parameters $p(\boldsymbol{\beta}, \boldsymbol{\theta})$, where these priors are assumed to be independent (i.e., $p(\boldsymbol{\beta}, \boldsymbol{\theta}) = p(\boldsymbol{\beta})p(\boldsymbol{\theta})$) and noninformative (see Appendix B for more details on the priors used). All inference for $\boldsymbol{\beta}$ and $\boldsymbol{\theta}$ is based on the marginalized posterior for these parameters conditional on \mathbf{z}_O :

$$p(\boldsymbol{\beta}, \boldsymbol{\theta} | \mathbf{z}_O) \propto p(\mathbf{z}_O | \boldsymbol{\beta}, \boldsymbol{\theta}) p(\boldsymbol{\beta}) p(\boldsymbol{\theta}). \quad (6)$$

Regardless of the form of the priors on $\boldsymbol{\beta}$ and $\boldsymbol{\theta}$, the posterior distribution (6) is not available in closed form, and so we must resort to Markov chain Monte Carlo (MCMC) methods to conduct inference on $\boldsymbol{\beta}$ and $\boldsymbol{\theta}$. Providing methods for sampling from this posterior for a variety of covariance models is the objective of this software package.

Posterior prediction of the process $y(\cdot)$ for either the observed locations \mathcal{S}_O or a distinct set of M unobserved locations $\mathcal{S}_P = \{\mathbf{s}_1^*, \dots, \mathbf{s}_M^*\} \in G$ is straightforward given the Gaussian process assumptions used here. Define $\mathbf{y}_P = (y(\mathbf{s}_1^*), \dots, y(\mathbf{s}_M^*))^\top$ and $\mathbf{y} = (\mathbf{y}_O, \mathbf{y}_P)$; the predictive distribution of interest is then

$$p(\mathbf{y} | \mathbf{z}_O) = \int_{\boldsymbol{\beta}, \boldsymbol{\theta}} p(\mathbf{y}, \boldsymbol{\beta}, \boldsymbol{\theta} | \mathbf{z}_O) d\boldsymbol{\beta} d\boldsymbol{\theta} = \int_{\boldsymbol{\beta}, \boldsymbol{\theta}} p(\mathbf{y} | \boldsymbol{\beta}, \boldsymbol{\theta}, \mathbf{z}_O) p(\boldsymbol{\beta}, \boldsymbol{\theta} | \mathbf{z}_O) d\boldsymbol{\beta} d\boldsymbol{\theta}. \quad (7)$$

The first component inside the integral on the far right hand side of (7), i.e., $p(\mathbf{y} | \boldsymbol{\beta}, \boldsymbol{\theta}, \mathbf{z}_O)$, is available in closed form. The Gaussian process assumption yields that the joint distribution of $(\mathbf{z}_O, \mathbf{y})$ conditional on $(\boldsymbol{\beta}, \boldsymbol{\theta})$ is

$$p\left(\begin{bmatrix} \mathbf{z}_O \\ \mathbf{y} \end{bmatrix} \middle| \boldsymbol{\beta}, \boldsymbol{\theta}\right) = N\left(\begin{bmatrix} \mathbf{X}_O \boldsymbol{\beta} \\ \mathbf{X} \boldsymbol{\beta} \end{bmatrix}, \begin{bmatrix} \mathbf{C}_{\mathbf{z}_O} & \mathbf{C}_{\mathbf{z}_O, \mathbf{y}} \\ \mathbf{C}_{\mathbf{y}, \mathbf{z}_O} & \mathbf{C}_{\mathbf{y}} \end{bmatrix}\right)$$

(implicit conditioning on $\boldsymbol{\theta}$ on the right hand side suppressed), where the entries of the covariance (or cross-covariance) matrices $\mathbf{C}_{(\cdot)}$ are determined from the covariance functions $C_{(\cdot)}$. Based on the conditional properties of the multivariate Gaussian distribution, we have

$$p(\mathbf{y} | \mathbf{z}_O, \boldsymbol{\beta}, \boldsymbol{\theta}) = N(\mathbf{m}_{\mathbf{y} | \mathbf{z}_O}, \mathbf{C}_{\mathbf{y} | \mathbf{z}_O}),$$

where

$$\mathbf{m}_{\mathbf{y}|\mathbf{z}_O} = \mathbf{X}\boldsymbol{\beta} + \mathbf{C}_{\mathbf{y},\mathbf{z}_O} \mathbf{C}_{\mathbf{z}_O}^{-1}(\mathbf{z}_O - \mathbf{X}_O\boldsymbol{\beta})$$

and

$$\mathbf{C}_{\mathbf{y}|\mathbf{z}_O} = \mathbf{C}_{\mathbf{y}} - \mathbf{C}_{\mathbf{y},\mathbf{z}_O} \mathbf{C}_{\mathbf{z}_O}^{-1} \mathbf{C}_{\mathbf{y},\mathbf{z}_O}.$$

The other component under the integral on the far right hand side of (7) is the posterior (6); hence, in practice, given a set of posterior samples $\{\boldsymbol{\beta}_l, \boldsymbol{\theta}_l : l = 1, \dots, L\}$ (obtained via MCMC), a Monte Carlo estimate of (7) is obtained via

$$p(\mathbf{y}|\mathbf{z}_O) \approx \sum_{l=1}^L p(\mathbf{y}|\mathbf{z}_O, \boldsymbol{\beta}_l, \boldsymbol{\theta}_l).$$

3 Nonstationary covariance function modeling

Among the diverse literature on approaches for modeling a nonstationary covariance function, one of the more intuitive methods involves allowing the parameters of the covariance function C_y to vary over space, the so-called spatially-varying parameters approach. Following Paciorek and Schervish (2006), Risser and Calder (2015), and many others, one approach for modeling the parametric covariance function for $y(\cdot)$ is via

$$C_y(\mathbf{s}, \mathbf{s}'; \boldsymbol{\theta}) = \sigma(\mathbf{s})\sigma(\mathbf{s}') \frac{|\boldsymbol{\Sigma}(\mathbf{s})|^{1/4} |\boldsymbol{\Sigma}(\mathbf{s}')|^{1/4}}{\left| \frac{\boldsymbol{\Sigma}(\mathbf{s}') + \boldsymbol{\Sigma}(\mathbf{s})}{2} \right|^{1/2}} \mathcal{M}_\nu \left(\sqrt{Q(\mathbf{s}, \mathbf{s}')} \right), \quad \mathbf{s}, \mathbf{s}' \in G \quad (8)$$

where

$$Q(\mathbf{s}, \mathbf{s}') = (\mathbf{s} - \mathbf{s}')^\top \left(\frac{\boldsymbol{\Sigma}(\mathbf{s}) + \boldsymbol{\Sigma}(\mathbf{s}')}{2} \right)^{-1} (\mathbf{s} - \mathbf{s}') \quad (9)$$

and $\mathcal{M}_\nu(\cdot)$ is the Matérn correlation function with smoothness ν (note, however, that C_y is non-negative definite for any valid correlation function over \mathcal{R}^d , $d \geq 1$). In (8), $\sigma(\cdot)$ is a spatially-varying standard deviation process and $\boldsymbol{\Sigma}(\cdot)$ is a spatially-varying anisotropy process that controls the range and direction of dependence. The covariance function in Eq. 8 arises as a generalization of a kernel convolution-based approach for constructing a positive definite covariance function (e.g., Higdon et al., 1999); see Paciorek and Schervish (2006) for further details.

The covariance function defined via (5) and (8) is highly flexible, as it defines parameter processes $\sigma(\cdot)$ and $\boldsymbol{\Sigma}(\cdot)$ —and $\tau(\cdot)$, the standard deviation process for the error $\varepsilon(\cdot)$, when considering C_z —over an infinite-dimensional space (i.e., $G \subset \mathcal{R}^d$). In practice, these processes must be regularized somehow so that implementation is feasible. We outline a variety of approaches for parameterizing and regularizing these processes, all of which involve modeling the parameter processes as spatially-varying fields.

3.1 Scalar standard deviation processes

The processes $\tau(\cdot)$ and $\sigma(\cdot)$ represent standard deviations for the error $\varepsilon(\cdot)$ and process $y(\cdot)$, respectively, and by definition are strictly positive. A variety of models can be specified for

scalar (i.e., univariate) spatial processes defined on the positive real line. Several are outlined below.

3.1.1 Spatial constants

While the main point of the methods in this paper is to allow the variance/covariance properties to vary over space, for completeness we also define spatially-constant error and spatial standard deviations:

$$\tau(\mathbf{s}) \equiv \delta, \quad \sigma(\mathbf{s}) \equiv \alpha \quad \text{for all } \mathbf{s} \in G \quad (10)$$

3.1.2 Log-linear regression

The simplest approach for modeling spatially-varying $\tau(\cdot)$ and $\sigma(\cdot)$ is a regression model that is linear in a set of spatial covariates on the log scale, i.e.,

$$\log \tau(\mathbf{s}) = \mathbf{x}_\tau(\mathbf{s})^\top \boldsymbol{\delta}, \quad \log \sigma(\mathbf{s}) = \mathbf{x}_\sigma(\mathbf{s})^\top \boldsymbol{\alpha}, \quad (11)$$

where $\mathbf{x}_{(\cdot)}(\mathbf{s}) \in \mathcal{R}^{p(\cdot)}$ is a set of fully-observed covariates (including an intercept) and $\boldsymbol{\delta}$ and $\boldsymbol{\alpha}$ are vectors of regression coefficients. This is likely the most parsimonious representation of the process, as it involves only $p(\cdot)$ parameters. Note that in this framework, $\mathbf{x}_{(\cdot)}(\mathbf{s})$ could represent either physical covariates (for a spatial process, e.g., orography or land use categories) or basis functions (e.g., empirical orthogonal functions or EOFs).

3.1.3 Approximation to a stationary Gaussian process

While the regression framework is highly parsimonious, it specifies a rigid relationship between the processes $\tau(\cdot)$ and $\sigma(\cdot)$ and the choice of covariates. Furthermore, as is often a challenge in spatial regression, the covariate vector must be fully observed over the spatial domain, including any prediction location of interest. An additional degree of flexibility can be gained by modeling either $\tau(\cdot)$ or $\sigma(\cdot)$ as itself a stationary Gaussian process with Matérn covariance. For simplicity of notation, in the remainder of this section we generically use ϕ to represent either standard deviation process. So, for $\phi \in \{\tau, \sigma\}$, we can model

$$\log \phi(\mathbf{s}) \sim GP(\mu_\phi, C_\phi(\cdot; \rho_\phi, \sigma_\phi, \nu_\phi)), \quad (12)$$

where $E[\phi(\mathbf{s})] = \mu_\phi$ and C_ϕ is the stationary Matérn covariance function with standard deviation σ_ϕ , spatial range ρ_ϕ , and smoothness ν_ϕ . [Paciorek and Schervish \(2004\)](#) use this statistical model for the anisotropy components (see Section 3.2), but [Paciorek and Schervish \(2006\)](#) found the MCMC computations to be slow (likely due to the fact that the parameter space for the model in Eq. 12 is of dimension $N + 4$). As an alternative, [Paciorek and Schervish \(2006\)](#) suggest using a basis function approximation to a stationary Gaussian process ([Kammann and Wand, 2003](#)), again originally specified for the anisotropy components, in which the vector of values $\boldsymbol{\phi} = (\phi(\mathbf{s}_1), \dots, \phi(\mathbf{s}_n))$ is modeled as a linear combination of basis functions:

$$\log \boldsymbol{\phi} = \mu_\phi \mathbf{1}_N + \sigma_\phi \mathbf{P}_\phi \mathbf{V}_\phi^{-1/2} \mathbf{w}_\phi \quad (13)$$

In (13), \mathbf{w}_ϕ is a latent process defined on a set of knot locations $\{\mathbf{b}_k : k = 1, \dots, K\}$, the radial basis functions $\mathbf{P}_\phi \mathbf{V}_\phi^{-1/2}$ are constructed using the $N \times K$ matrix of pairwise Matérn

correlations $C_\phi(\cdot; \rho_\phi, \nu_\phi)$ between the observation locations and knot locations (\mathbf{P}_ϕ) and the inverse square root of the $K \times K$ matrix of pairwise Matérn correlations among the knot locations (\mathbf{V}_ϕ). If the knots correspond to the observation locations, this representation would correspond exactly with that in (12). The vector of unknown parameters includes \mathbf{w}_ϕ as well as $\{\mu_\phi, \rho_\phi, \sigma_\phi, \nu_\phi\}$, but the dimension of the parameter space is now only $K + 4$. Note that some of the hyperparameters $\{\mu_\phi, \rho_\phi, \sigma_\phi, \nu_\phi\}$ might need to be fixed (see, e.g., Paciorek and Schervish, 2006, Section 3.2.2). Again, note that Paciorek and Schervish (2006) use this approach for the scalar anisotropy components, but here we propose using the same statistical model for variance components.

Note that there is a correspondence between (13) and the mixture component approach used in Risser and Calder (2017): certain values of the hyperparameters $\{\mu_\phi, \rho_\phi, \sigma_\phi, \nu_\phi\}$ in (13) make the two approaches (essentially) equivalent. For this paper we only include the approach given in Paciorek and Schervish (2006).

3.2 Matrix-valued anisotropy process

The anisotropy process $\Sigma(\cdot)$ is defined over the space of $d \times d$ positive definite matrices. As such, it is less straightforward how to specify a process model for $\Sigma(\cdot)$. Several approaches are described in the following sections.

3.2.1 Spatial constant

Again, for completeness we define a spatially-constant anisotropy process:

$$\Sigma(\mathbf{s}) \equiv \Sigma, \quad \text{for all } \mathbf{s} \in G \quad (14)$$

3.2.2 Covariance regression

Using the intuition from mean regression, Risser and Calder (2015) use covariance regression (Hoff and Niu, 2012) to parameterize the anisotropy process. Specifically,

$$\Sigma(\mathbf{s}) = \Psi + \Gamma \mathbf{x}_\Sigma(\mathbf{s}) \mathbf{x}_\Sigma(\mathbf{s})^\top \Gamma^\top, \quad (15)$$

where $\mathbf{x}_\Sigma(\mathbf{s}) \in \mathcal{R}^{p_\Sigma}$ is a vector of relevant covariates (including an intercept, of length p_Σ), Ψ is a $d \times d$ positive definite matrix, Γ is a $d \times p_\Sigma$ real matrix. Because Ψ is positive definite, the number of parameters in this representation is $d(d+1)/2 + dp_\Sigma$.

3.2.3 Componentwise regression

Alternatively, one might decompose the anisotropy process $\Sigma(\cdot)$ into the $d(d+1)/2$ unique processes. For example, Paciorek and Schervish (2006) suggest the eigendecomposition

$$\Sigma(\mathbf{s}) = \Gamma(\mathbf{s}) \Lambda(\mathbf{s}) \Gamma(\mathbf{s})^\top,$$

where $\Lambda(\cdot)$ is a diagonal matrix of eigenvalues and $\Gamma(\cdot)$ is a matrix of eigenvectors. Even in this representation, there are many ways to parameterize the unique parameters of each $\Sigma(\cdot)$ (see, e.g. Paciorek and Schervish, 2006); for $d = 2$, we use

$$\mathbf{\Lambda}(\mathbf{s}) = \begin{bmatrix} \lambda_1(\mathbf{s}) & 0 \\ 0 & \lambda_2(\mathbf{s}) \end{bmatrix}, \quad \mathbf{\Gamma}(\mathbf{s}) = \begin{bmatrix} \cos \gamma(\mathbf{s}) & -\sin \gamma(\mathbf{s}) \\ \sin \gamma(\mathbf{s}) & \cos \gamma(\mathbf{s}) \end{bmatrix}, \quad (16)$$

as in [Risser and Calder \(2015\)](#), where we limit $\gamma(\mathbf{s}) \in [0, \frac{\pi}{2}]$ for identifiability. Now, in terms of $\lambda_1(\mathbf{s})$, $\lambda_2(\mathbf{s})$, and $\gamma(\mathbf{s})$, we can define linear regression models on transformed versions of these parameters:

$$\begin{aligned} \log \lambda_1(\mathbf{s}) &= \mathbf{x}_\Sigma(\mathbf{s})^\top \boldsymbol{\alpha}_{\lambda_1} \\ \log \lambda_2(\mathbf{s}) &= \mathbf{x}_\Sigma(\mathbf{s})^\top \boldsymbol{\alpha}_{\lambda_2} \\ \log \frac{\frac{2}{\pi}\gamma(\mathbf{s})}{1-\frac{2}{\pi}\gamma(\mathbf{s})} &= \mathbf{x}_\Sigma(\mathbf{s})^\top \boldsymbol{\alpha}_\gamma, \end{aligned} \quad (17)$$

where the transformations are such that each component has real support.

3.2.4 Nonparametric regression

Using the decomposition into three scalar processes given in (16), we could also apply the approximate GP representation in (13) to each of $\{\log \lambda_1(\cdot), \log \lambda_2(\cdot), \log \frac{\frac{2}{\pi}\gamma(\cdot)}{1-\frac{2}{\pi}\gamma(\cdot)}\}$. Aside from their alternate parameterization, this is the approach used in [Paciorek and Schervish \(2006\)](#).

3.2.5 Local isotropy

For spatial dimensions larger than $d = 2$, estimating a spatially-varying anisotropy process becomes more challenging due to the large number of parameters needed to model the $d(d+1)/2$ unique processes in $\Sigma(\mathbf{s})$. One (albeit simplified) way around this problem is to force the covariance to be locally isotropic by setting the anisotropy process to be equal to a multiple of the identity matrix:

$$\Sigma(\mathbf{s}) \equiv \Sigma(\mathbf{s})\mathbf{I}_d,$$

where $\Sigma(\mathbf{s})$ is a scalar. In this case, Equations (8) and (9) become

$$Q(\mathbf{s}, \mathbf{s}') = \frac{(\mathbf{s} - \mathbf{s}')^\top (\mathbf{s} - \mathbf{s}')}{\frac{1}{2}[\Sigma(\mathbf{s}) + \Sigma(\mathbf{s}')] } = \frac{\|\mathbf{s} - \mathbf{s}'\|^2}{\frac{1}{2}[\Sigma(\mathbf{s}) + \Sigma(\mathbf{s}')] },$$

and

$$C_y(\mathbf{s}, \mathbf{s}'; \boldsymbol{\theta}) = \sigma(\mathbf{s})\sigma(\mathbf{s}') \frac{(\Sigma(\mathbf{s})\Sigma(\mathbf{s}'))^{d/4}}{\left(\frac{\Sigma(\mathbf{s}) + \Sigma(\mathbf{s}')}{2}\right)^{d/2}} g\left(\sqrt{Q(\mathbf{s}, \mathbf{s}')}\right), \quad \mathbf{s}, \mathbf{s}' \in G. \quad (18)$$

Note that now $Q(\mathbf{s}, \mathbf{s}')$ (and hence C_y) only depends on the squared Euclidean distances $\|\mathbf{s} - \mathbf{s}'\|^2$. In this case, we can apply any of the componentwise and nonparametric regression frameworks to $\log \Sigma(\mathbf{s})$ to estimate the nonstationary (but locally isotropic) covariance function in (18) for an arbitrary spatial dimension $d \geq 1$.

4 Approximate inference and prediction for large data

Despite the fact that Gaussian processes are mathematically convenient representations for a spatial process and that prediction is straightforward, numerical calculations regarding

the multivariate Gaussian distribution for N spatial locations require $\mathcal{O}(N^2)$ memory and $\mathcal{O}(N^3)$ time complexity. This is an issue for any application of Gaussian processes, but is particularly problematic for modeling nonstationary covariance functions which involve high-dimensional parameter spaces. When posterior prediction is necessary, the computational complexity is even worse for large M . However, when dealing with large data sets, we can utilize the diverse literature on approximate Gaussian process methods (see [Heaton et al., 2018](#), for a review and comparison of existing approaches) to make parameter inference and prediction feasible.

The nearest-neighbor Gaussian process (NNGP; [Datta et al., 2016](#)) and the sparse general Vecchia (SGV; [Katzfuss and Guinness, 2017](#) and [Katzfuss et al., 2018](#)) approximations are two specific methods that enable large data inference via Gaussian processes by forcing the precision matrix to be sparse. Actually, both of these methods can be seen as special cases of Vecchia approximations of Gaussian processes ([Katzfuss and Guinness, 2017](#)); we introduce both using a single framework but later describe them distinctly (our reasons for doing so will become clear later in this section). For now focusing on the distribution of the latent process $y(\cdot)$ at the observed locations \mathcal{S}_O , note that we can write (3) as

$$p(\mathbf{y}_O) = p(y_1) \prod_{i=2}^N p(y_i | \mathbf{y}_{h(i)}) \quad (19)$$

(implicit conditioning on $\boldsymbol{\theta}$ and $\boldsymbol{\beta}$ suppressed for simplicity), where we denote $y_i = y(\mathbf{s}_i)$, $h(i) = (1, \dots, i-1)$, and $\mathbf{y}_{h(i)} = \{y_j : j \in h(i)\}$; note that in this framework the ordering of the locations in \mathcal{S}_O is assumed to be arbitrarily fixed. However, (19) provides no computational shortcuts, as the conditional densities still involve $\mathcal{O}(N^2)$ memory and $\mathcal{O}(N^3)$ computations. To navigate these limitations, Vecchia’s approximation ([Vecchia, 1988](#)) suggests an approximation to (19) wherein the conditioning sets $h(i)$ are replaced with subvectors $g(i) \subset h(i)$, where $g(i)$ usually refers to the indices that are “near” \mathbf{s}_i . We utilize terminology from [Katzfuss and Guinness \(2017\)](#) and refer to $g(i)$ as the i th conditioning index vector and $\mathbf{y}_{g(i)}$ as the conditioning vector for y_i , yielding the Vecchia approximation of the joint density in (19):

$$\hat{p}(\mathbf{y}_O) = p(y_1) \prod_{i=2}^N p(y_i | \mathbf{y}_{g(i)}) \quad (20)$$

The Vecchia approximation (20) converges to the true distribution in (19) as the conditioning vectors $g(i)$ approach $h(i)$, but of course we prefer small conditioning vectors for computational efficiency.

A more general framework applies to the vector $\mathbf{w}_O = \mathbf{y}_O \cup \mathbf{z}_O$, where (again following notation from [Katzfuss and Guinness, 2017](#)) the ordering in \mathbf{w}_O is such that the y_i retain their relative ordering in \mathbf{w}_O and the z_i are inserted directly after y_i . The general Vecchia approximation ([Katzfuss and Guinness, 2017](#)) is defined as

$$\hat{p}(\mathbf{w}_O) = \prod_{i=1}^N p(w_i | \mathbf{w}_{g(i)}) \quad (21)$$

(where we now define $g(1) = \emptyset$), which can also be written as

$$\hat{p}(\mathbf{w}_O) = \prod_{i=1}^N \left[p(y_i | \mathbf{y}_{q_y(i)}, \mathbf{z}_{q_z(i)}) \times p(z_i | y_i) \right]. \quad (22)$$

The conditioning vector for z_i is always y_i because (1) assumes z_i is conditionally independent of all other observed responses given y_i . In the general form written in (22), the conditioning vector for y_i has been split into two sub-vectors $q_y(i)$ and $q_z(i)$, where $j \in q_y(i)$ means y_i conditions on y_j and $j \in q_z(i)$ means y_i conditions on z_j (in other words, does y_i condition on the latent or observed value). Finally, we assume $q_y(i) \cap q_z(i) = \emptyset$ and denote $q(i) = (q_y(i), q_z(i))$.

Katzfuss and Guinness (2017) state that a general Vecchia approximation $\hat{p}(\mathbf{w}_O)$ of $p(\mathbf{w}_O)$ is determined by several choices:

1. The ordering of the locations in \mathcal{S}_O ,
2. For each i , the conditioning index vector $q(i) \subset (1, \dots, i-1)$ for y_i , and
3. For each i , partitioning $q(i)$ into $q_y(i)$ and $q_z(i)$.

(Note that Katzfuss and Guinness, 2017 further describe the choice of a superset of the observations and a partitioning the superset; we simply use default choices of setting the superset equal to \mathcal{S}_O and using a scalar partitioning.) Regarding the first choice, we use an approximate maximum-minimum-distance (maxmin) ordering (Guinness, 2018), which has been shown as optimal for $d \geq 2$ dimensional spatial domains (Katzfuss and Guinness, 2017). Regarding the second choice, we use k nearest-neighbor (NN) conditioning, i.e., $q(i) = (1, \dots, i-1)$ for $i \leq k$ and $q(i)$ consists of the k locations from $(1, \dots, i-1)$ with the smallest Euclidean distance from \mathbf{s}_i otherwise. The third choice has a greater impact on the computational properties of the resulting Vecchia approximation (22), and we present two cases in Sections 4.1 (sparse general Vecchia or SGV) and 4.2 (nearest neighbor GP for the response or NNGP-R). As mentioned at the beginning of the section, inference for both cases could be presented in a single framework (which is the organization in Katzfuss and Guinness, 2017), but here we present things separately given computational differences in the resulting implementation.

4.1 Sparse general Vecchia

The sparse general Vecchia (SGV) approximation (Katzfuss and Guinness, 2017) is defined by a particular partitioning of the conditioning index vector: for each i , partition $q(i)$ into $q_y(i)$ and $q_z(i)$ such that j and l with $j < l$ can only both be in $q_y(i)$ if $j \in q_y(l)$. The SGV partitioning ensures that the corresponding directed acyclic graph forms a “perfect graph” (Lauritzen, 1996). Following Katzfuss and Guinness (2017), we obtain $q_y(i)$ for each $i = 2, \dots, N$ as

$$q_y(i) = (l_i) \cup ((q_y(l_i) \cap q(i))),$$

where l_i is the index in $\arg \max_{j \in q(i)} |q_y(j) \cap q(i)|$ for which the spatial distance between \mathbf{s}_i and \mathbf{s}_{l_i} is the shortest. The SGV partitioning provides a compromise between conditioning

only on the $y(\cdot)$ (which provides a better approximation but is slower computationally) and only on $z(\cdot)$ (which provides a worse approximation but is much faster; see Section 4.2).

The general Vecchia approximation implied by (22) is the multivariate Gaussian distribution $N_n(\boldsymbol{\mu}_O, \boldsymbol{\Sigma}_O)$. The SGV guarantees that both $\boldsymbol{\Sigma}_O^{-1}$ and \mathbf{U}_O are sparse, where

$$\boldsymbol{\Sigma}_O^{-1} = \mathbf{U}_O \mathbf{U}_O^\top$$

and \mathbf{U}_O is the upper triangular Cholesky factor based on a reverse row-column ordering of $\boldsymbol{\Sigma}_O^{-1}$ (Katzfuss and Guinness, 2017). For a known covariance function and a fixed value of the covariance parameters, a closed form expression is available for the non-zero elements of \mathbf{U}_O (Proposition 1, Katzfuss and Guinness, 2017); thus, \mathbf{U}_O has at most $k + 1$ nonzero entries per column, such that \mathbf{U}_O can be computed in $\mathcal{O}(Nk^3)$ time (Katzfuss and Guinness, 2017). Note that the elements of \mathbf{U}_O corresponding to \mathbf{y}_O are based on C_y (from Eq. 8); the elements corresponding to \mathbf{z}_O are a function of the error process variance process $\tau(\cdot)$.

The likelihood corresponding to the $N(\boldsymbol{\mu}_O, \boldsymbol{\Sigma}_O)$ density can be computed as follows: define submatrices \mathbf{A}_O and \mathbf{B}_O consisting of the rows of \mathbf{U}_O corresponding to \mathbf{y}_O and \mathbf{z}_O , respectively. Furthermore, define \mathbf{W}_O to be the submatrix of $\boldsymbol{\Sigma}_O^{-1}$ corresponding to \mathbf{y}_O , computed as $\mathbf{W}_O = \mathbf{A}_O \mathbf{A}_O^\top$, and define \mathbf{V}_O to be the upper triangular Cholesky factor based on a reverse row-column ordering of \mathbf{W}_O . Integrating $\hat{p}(\mathbf{w}_O)$ with respect to \mathbf{y}_O results in the approximate log-likelihood

$$\begin{aligned} \log \hat{p}(\mathbf{z}_O) \propto & - \sum_{i=1}^N \log U_{ii} + \sum_{i=1}^N \log V_{ii} - \frac{1}{2}(\mathbf{z} - \boldsymbol{\mu}_O)^\top \mathbf{B}_O \mathbf{B}_O^\top (\mathbf{z} - \boldsymbol{\mu}_O) \\ & + \frac{1}{2}(\mathbf{z} - \boldsymbol{\mu}_O)^\top \mathbf{B}_O \mathbf{A}_O^\top (\mathbf{V}_O^{-1})^\top \mathbf{V}_O^{-1} \mathbf{A}_O \mathbf{B}_O^\top (\mathbf{z} - \boldsymbol{\mu}_O) \end{aligned} \quad (23)$$

(Katzfuss and Guinness, 2017). Because the time complexity for computing \mathbf{V}_O is $\mathcal{O}(Nk^2)$ (Katzfuss and Guinness, 2017, Proposition 6), the SGV approximation retains linear computational complexity in N . However, in practice, note that calculating (23) efficiently requires sparse matrix operations (using, e.g., the **Matrix** package in R), since this framework for deriving the conditioning index vectors does not allow (23) to be simplified any further.

Prediction in the SGV approach can be framed as a post-processing step when adopting an ordering scheme that first orders the observed locations and then orders the prediction locations (the so-called “obs-pred” ordering; see Katzfuss et al., 2018). While this restricts the choice of ordering somewhat, the primary benefit is that under obs-pred ordering the approximate likelihood for just \mathbf{w}_O is equal to the marginalized likelihood of the combined vector $(\mathbf{w}_O, \mathbf{y}_P)$ (integrated with respect to \mathbf{y}_P); thus, likelihood inference can first be carried out based on just \mathbf{w}_O and then \mathbf{y}_P can be appended when predictions are desired, without changing the distribution $\hat{p}(\mathbf{w}_O)$ (Katzfuss et al., 2018). Using similar notation as above, now define \mathbf{U} to be the Cholesky of the joint vector $(\mathbf{w}_O, \mathbf{y}_P)$, with \mathbf{A} and \mathbf{B} the corresponding submatrices of \mathbf{U} consisting of the rows of $(\mathbf{y}_O, \mathbf{y}_P)$ and \mathbf{z}_O , respectively, and finally \mathbf{V} to be the Cholesky factor based on a reverse row-column ordering of $\mathbf{W} = \mathbf{A} \mathbf{A}^\top$. Then, for a fixed value of the mean and covariance parameters, the posterior mean of $\mathbf{y} = (\mathbf{y}_O, \mathbf{y}_P)$ is

$$\boldsymbol{\mu}_{\text{post,SGV}} = \mathbf{X}\boldsymbol{\beta} - (\mathbf{V}^\top)^{-1} \mathbf{V}^{-1} \mathbf{A} \mathbf{B}^\top (\mathbf{z}_O - \mathbf{X}_O \boldsymbol{\beta})$$

(where the design matrices are ordered appropriately), and a draw from the conditional posterior of can be computed as $\mathbf{y}^* = \boldsymbol{\mu}_{\text{post,SGV}} + (\mathbf{V}^\top)^{-1}\mathbf{g}$, where $g_i \stackrel{iid}{\sim} N(0, 1)$ (Katzfuss et al., 2018). As with likelihood inference, predictions for SGV under obs-pred ordering can be obtained in $\mathcal{O}(Nk)$ time complexity, which is linear in N .

4.2 Nearest Neighbor Gaussian Process-Response

The nearest neighbor Gaussian process for the response (Finley et al., 2018) can be seen as a special case of the general Vecchia approximation where the conditioning index vector for all y_i includes only elements of the observed \mathbf{z}_O ; i.e., $q_y(i) = \emptyset$. Given that the NNGP-R approximation is a special case of the general Vecchia approximation, likelihood calculations could be conducted as with SGV. However, given the conditioning structure, with NNGP-R one can explicitly integrate over the \mathbf{y}_O and apply the likelihood approximation directly to $p(\mathbf{z}_O)$ (from Eq. 4; conditioning on mean and covariance parameters suppressed), whereas the general Vecchia framework specifies an approximation to $p(\mathbf{w}_O) = p(\mathbf{y}_O, \mathbf{z}_O)$. The NNGP-R approximation is now applied to yield a sparse Cholesky factor of $\text{Cov}(\mathbf{z}_O)$, which is based on C_z (from Eq. 5), as opposed to the general Vecchia which calculates the sparse Cholesky factor of $\text{Cov}(\mathbf{y}_O, \mathbf{z}_O)$ based on C_y and $\tau(\cdot)$. Furthermore, Finley et al. (2018) derive a closed form expression for calculating the Cholesky factor of $\text{Cov}(\mathbf{z}_O)$ and the subsequent quadratic forms needed to evaluate the likelihood. When the number of nonzero elements in the Cholesky decomposition is limited to k (again using a k nearest neighbor scheme based on maxmin ordering), the Cholesky is guaranteed to be sparse and can be calculated by solving $N - 1$ linear systems of size at most $k \times k$, which can be performed in $\mathcal{O}(Nk^3)$ flops (furthermore, parallelization could be employed, since each linear system can be solved independently of all others). As such, the likelihood can then be calculated in $\mathcal{O}(Nk)$ time complexity (Finley et al., 2018), which is linear in N .

The tradeoff of conditioning on the observed \mathbf{z}_O is that posterior prediction can only be accomplished for individual locations (also called “local kriging”) because the covariance corresponding to the prediction locations is diagonal (Section 5.2.1 of Katzfuss et al., 2018). Finley et al. (2018) outline an algorithm for posterior prediction of the response (i.e., $z(\cdot)$) at a single location (Algorithm 4, Finley et al., 2018); Katzfuss et al. (2018) note that the same framework can be used to predict either $z(\cdot)$ or $y(\cdot)$ by including or not including the nugget variance, respectively, in the prediction variance. Therefore, while the joint posterior mean for a set of independent predictions over \mathcal{S}_P will have the right spatial structure, individual draws from the posterior will be spatially independent.

4.3 Comparing SGV and NNGP-R

In summary, while the SGV and NNGP-R approximations both arise as special cases of the general Vecchia approximation, there are important differences in the underlying properties of the resulting approximation. First, the approximation accuracy is better for SGV, relative to NNGP-R (Proposition 4 in Katzfuss et al., 2018). However, Katzfuss et al. (2018) show empirically that both likelihood calculations and prediction are much faster for NNGP-R relative to SGV (Figure 5, Katzfuss et al., 2018). SGV performs better in the low signal-to-noise situation; also, SGV can characterize joint predictions whereas NNGP-R can only

yield marginal (univariate) predictions. This last feature is potentially the most problematic; as stated in [Katzfuss et al. \(2018\)](#), “joint predictive distributions are crucial for accurate uncertainty quantification for spatial averages or totals. For example, climate scientists are interested in obtaining uncertainties on the global average temperature, and hydrologists may wish to quantify uncertainty in total rainfall in a catchment area.” This important trade-off between computational speed and approximation accuracy/joint prediction is the primary reason why we have chosen to include both of these methods in this paper (and the corresponding software package), as the specific application may motivate a preference for speed vs. accuracy, and furthermore if joint predictions are required or not.

5 Implementation

The **BayesNSGP** package (version 0.1.1) is available on CRAN (Comprehensive R Archive Network), the central repository for curating and disseminating R packages ([Hornik, 2012](#)). The methods outlined in Sections 2, 3, and 4 are implemented in the two outward-facing user interface functions, `nsgrpModel` and `nsgrpPredict`. These functions respectively fit a Bayesian spatial Gaussian process and generate posterior predictions for a set of locations. Details on how to use these functions is described in the following sections. Note that documentation of the other (helper) functions are provided within the **BayesNSGP** package, but explicit descriptions are omitted here for brevity and simplicity.

5.1 nsgrpModel: MCMC for a general nonstationary spatial GP

The primary arguments of `nsgrpModel` (and their default settings) are

```
nsgrpModel( tau_model = "constant", sigma_model = "constant",
  Sigma_model = "constant", mu_model = "constant", likelihood = "fullGP",
  coords, data, constants = list(), monitorAllSampledNodes = TRUE, ... )
```

The structure of a particular spatial model is defined by choices of `tau_model`, `sigma_model`, `Sigma_model`, and `mu_model`, which respectively specify statistical models for $\tau(\cdot)$, $\sigma(\cdot)$, $\Sigma(\cdot)$, and the mean of the process $\mu(\cdot)$. Any or all of the parameter processes can utilize the various statistical models outlined in Section 3; the syntax for each option is given in Appendix B (e.g., `tau_model = "logLinReg"` uses log-linear regression for the $\tau(\cdot)$ process). The `likelihood` argument specifies the likelihood to use—choosing from `"fullGP"` (the exact Gaussian likelihood), `"SGV"` (the sparse general Vecchia), or `"NNGP"` (the nearest-neighbor Gaussian process). The default is to fit a stationary Gaussian process with the exact GP likelihood (i.e., the parameter processes are all constant over space). Next, the `coords` argument takes the $N \times d$ matrix of spatial coordinates, and `data` is the N -vector of measurements. The `constants` argument is the most complicated input to the `nsgrpModel` function, as it contains all constants needed to be passed to the **nimble** package to build and compile the `nimbleModel` object, which will later be used to compile and run the Markov chain Monte Carlo. This list contains objects such as design matrices, fixed data-level hyperparameters, and fixed prior-level parameters. The tables in Appendix B contain the required constants for each likelihood/parameter process combination, as well as the default hyperparameter

values. The defaults are designed to be general, but we recommend that users explicitly set values of the hyperparameters for each data analysis. Note that one never needs to sample the latent process values (i.e., $y(\cdot)$) in an MCMC algorithm corresponding to a `nimbleModel` object, even for the SGV likelihood.

The `monitorAllSampledNodes` argument is used to specify which sampled parameters are stored in a given MCMC algorithm. The default value (`monitorAllSampledNodes = TRUE`) indicates that posterior samples will be recorded for both top-level model parameters and also for any latent states in the model. In our implementation of the **BayesNSGP** package, samples of the latent states are required for making predictions using the `nsgpPredict` function for certain submodels (specifically, when using the latent Gaussian process approach for either the variance or anisotropy processes). Overriding the default with `monitorAllSampledNodes = FALSE` specifies that posterior samples are recorded for *only* the top-level model parameters. This results in using far less memory and a subsequent decrease in execution speed, at the cost of not being able to conduct prediction at new locations. Note that one can also implement thinning in the execution of an MCMC algorithm to reduce storage considerations.

Finally, both `nsgpModel` and `nsgpPredict` were written in such a way that any constants provided in the `constants` list can also be provided as named arguments via the `...` argument. For example, the following two function calls are identical:

```
nsgpModel(coords = coords, data = data, constants = list(X_sigma = X,
  X_mu = X))
```

where two arguments are provided in the `constants` list and

```
nsgpModel(coords = coords, data = data, constants = list(), X_sigma = X,
  X_mu = X)
```

where the two components are provided as named arguments.

The object returned from `nsgpModel` is indeed a **nimble** “model” object, which is **nimble**’s abstraction for a hierarchical statistical model. **nimble** models provide the ability to store values into model parameters or latent states, designate values as observed data, simulate new values from prior distributions, and calculate log-densities. In addition, **nimble** algorithms (for example, **nimble**’s MCMC) natively operate on **nimble** model objects.

The general workflow is first creating a **nimble** model, then creating an MCMC algorithm to fit this model. The MCMC can optionally be customized, for example by assigning different samplers, such as slice sampling (Neal et al., 2003), Metropolis-Hastings sampling on a log scale for variance components, or joint sampling of correlated parameters using multivariate Metropolis-Hastings. Details of the sampling algorithms available with **nimble** can be found in R using `help(samplers)`, or in the **nimble** User Manual (<https://r-nimble.org/manuals/NimbleUserManual.pdf>). Once ready, both the model and MCMC are compiled to C++ (functionality provided by **nimble**) for faster execution. Finally, the compiled MCMC algorithm is executed to generate posterior samples.

In order to describe a generic implementation of the methods outlined in this paper, we consider a specific example involving a small, simulated data set, where the spatial coordinates are randomly sampled from the unit square. We further assume a mean that is linear in

the y -coordinate; a spatial variance that is log-linear in the x -coordinate; a constant nugget variance; and a constant anisotropy process. Finally, we use a smoothness of 0.5, i.e., we use the exponential correlation. (Note: the correlation matrix is calculated using the helper `nsCorr` function.)

```
R> # Setup
R> N <- 100
R> set.seed(0)
R> coords <- matrix(runif(2*N), ncol = 2)
R> Xmat1 <- cbind(rep(1,N),coords[,1])
R> Xmat2 <- cbind(rep(1,N),coords[,2])
R> mu_vec <- as.numeric(Xmat2 %*% c(0, 2)) # Mean
R> alpha_vec <- as.numeric(Xmat1 %*% c(-0.5, 1.5)) # Log process SD
R> dist_list <- nsDist(coords)
R> Cor_mat <- nsCorr( dist1_sq = dist_list$dist1_sq,
+   dist2_sq = dist_list$dist2_sq, dist12 = dist_list$dist12,
+   Sigma11 = rep(0.4, N), Sigma22 = rep(0.4, N),
+   Sigma12 = rep(0, N), nu = 0.5 )
R> Cov_mat <- diag(exp(alpha_vec)) %*% Cor_mat %*% diag(exp(alpha_vec))
R> D_mat <- diag(exp(rep(log(sqrt(0.05)), N))^2)
R> # Draw data
R> set.seed(1)
R> data <- as.numeric(mu_vec + t(chol(Cov_mat + D_mat)) %*% rnorm(N))
```

Suppose the we would like to fit a nonstationary model to this data set, using a log-linear regression model for $\sigma(\cdot)$ (linear in the y -coordinate), the isotropic version of componentwise regression for $\Sigma(\cdot)$ (linear in the x -coordinate), linear regression for $\mu(\cdot)$ (linear in the y -coordinate), and an approximate GP for $\tau(\cdot)$ (using the coordinates themselves as the knot locations). Furthermore, we will use the SGV likelihood with $k = 10$ neighbors. The required constants can be set up as

```
R> constants <- list( X_sigma = Xmat1, X_Sigma = Xmat2, X_mu = Xmat1,
+   tau_knot_coords = coords, k = 10 )
```

and we can build the model with

```
R> Rmodel <- nsgpModel( likelihood = "SGV", sigma_model = "logLinReg",
+   Sigma_model = "compRegIso", mu_model = "linReg", tau_model = "approxGP",
+   constants = constants, coords = coords, data = data )
```

Once the model has been built, the first step is to configure the MCMC:

```
R> conf <- configureMCMC(Rmodel)
```

The default samplers can be queried with:

```
R> conf$printSamplers()
[1] RW sampler: alpha[1]
```



```

[2] RW sampler: alpha[2]
[3] RW sampler: tauGP_mu
[4] RW sampler: tauGP_phi
[5] RW sampler: tauGP_sigma
[6] RW sampler: Sigma_coef1[1]
[7] RW sampler: Sigma_coef1[2]
[8] RW sampler: beta[1]
[9] RW sampler: beta[2]
[10] RW_block sampler: w_tau[1:100]

```

from which we can see that by default most parameters have been assigned univariate random walk samplers, except for the latent knot process values `w_tau[1:100]`, which have been assigned a large block random walk sampler. One of the main benefits of using **nimble** is that it is very easy to group univariate samplers into a single block sampler, or alternatively to swap in different sampler types. To fully reconfigure these default samplers, first remove the existing samplers via

```
R> conf$removeSamplers()
```

and then gradually reassign samplers as needed. For the sake of our example, we first assign adaptive block Metropolis Hastings random walk samplers to the spatial standard deviation regression coefficients (i.e., `alpha[1]` and `alpha[2]`), the mean regression coefficients (i.e., `beta[1]` and `beta[2]`), and the latent hyperparameters for the nugget standard deviation (i.e., `tauGP_mu`, `tauGP_phi`, and `tauGP_sigma`); then, we assign an automated factor slice sampler ([Tibbits et al., 2014](#)) to the anisotropy regression coefficients (i.e., `Sigma_coef1[1]` and `Sigma_coef1[2]`):

```

R> conf$addSampler(target = c("alpha[1]", "alpha[2]"), type = "RW_block")
R> conf$addSampler(target = c("beta[1]", "beta[2]"), type = "RW_block")
R> conf$addSampler(target = c("tauGP_mu", "tauGP_phi", "tauGP_sigma"),
+   type = "RW_block")
R> conf$addSampler(target = c("Sigma_coef1[1]", "Sigma_coef1[2]"),
+   type = "AF_slice")

```

Finally, in order to sample the latent process values `w_tau[1:100]`, a single large block random walk sampler is likely to be ineffective; on the other hand, a large number of univariate samplers (in this case, 100) will (1) slow down the MCMC and (2) be inefficient as these parameters are likely to display a large degree of posterior correlation. One way to navigate these difficulties is to use a compromise: use smaller block random walk samplers on spatial subsets of the parameter space. In this case, for example, we can separately sample blocks of the `w_tau[1:100]` values from each of four subdivisions of the unit square (splitting at 0.5 in each coordinate direction):

```

R> # First, subset the coordinates
R> groups <- list(which(coords[,1] < 0.5 & coords[,2] < 0.5))
R> groups[[2]] <- which(coords[,1] < 0.5 & coords[,2] >= 0.5)
R> groups[[3]] <- which(coords[,1] >= 0.5 & coords[,2] < 0.5)

```

```

R> groups[[4]] <- which(coords[,1] >= 0.5 & coords[,2] >= 0.5)
R> # Add block samplers
R> for(g in 1:4){
+   conf$addSampler(target = paste0("w_tau[", groups[[g]], "]"),
+   type = "RW_block")
+ }

```

To check the updated samplers, we can again query

```

R> conf$printSamplers()
[1] RW_block sampler: alpha[1], alpha[2]
[2] RW_block sampler: beta[1], beta[2]
[3] RW_block sampler: tauGP_mu, tauGP_phi, tauGP_sigma
[4] AF_slice sampler: Sigma_coef1[1], Sigma_coef1[2]
[5] RW_block sampler: w_tau[3], w_tau[15], w_tau[17], w_tau[20], ...
[6] RW_block sampler: w_tau[2], w_tau[6], w_tau[11], w_tau[12], ...
[7] RW_block sampler: w_tau[4], w_tau[7], w_tau[8], w_tau[9], ...
[8] RW_block sampler: w_tau[1], w_tau[5], w_tau[10], w_tau[18], ...

```

(note: the `w_tau` samplers have been shortened for brevity).

Once the samplers have been sufficiently modified, we can then build the MCMC, compile the model, and compile the MCMC as follows:

```

Rmcmc <- buildMCMC(conf) # Build the MCMC
Cmodel <- compileNimble(Rmodel) # Compile the model in C++
Cmcmc <- compileNimble(Rmcmc, project = Rmodel) # Compile the MCMC in C++

```

Finally, the MCMC can be run for, say, 20000 iterations (with 10000 discarded as burn-in and storing every fifth sample) using:

```

samples <- runMCMC(Cmcmc, niter = 20000, nburnin = 10000, thin = 5)

```

The `runMCMC` function is a **nimble** function designed to take an MCMC algorithm and run the MCMC with one or more chains, with optional arguments to burn-in or thin the output (for further information, we refer the reader to the **nimble** help files). The resulting `samples` object is a matrix with one row for each saved MCMC sample (2000 total, thinned from the 10000 post burn-in) and one column for each sampled parameter (109 in this case).

Three additional helper functions are necessary for setting up the required constants for the `nimbleModel` when using the SGV and NNGP likelihood models: `orderCoordinatesMMD`, `determineNeighbors`, and `sgvSetup`. All of these functions operate internally within a call of the `nsgrpModel` function, but it is important to understand what these functions are doing in the background. For both NNGP and SGV, the first step is to re-order the coordinates (and all corresponding quantities, e.g., the $z(\cdot)$ values, design matrices, etc.) following an approximate maximum-minimum distance (MMD; [Guinness, 2018](#)) ordering; this is accomplished using `orderCoordinatesMMD` (note that our implementation can calculate either an approximate MMD—the default—or an exact MMD, which is only recommended for very small data sets). Next, the approximate likelihood methods require a set of neighbors for

each location; `determineNeighbors` takes a set of spatial coordinates (of size $N \times d$) as well as the desired number of neighbors, k , and returns a $N \times k$ matrix indexing the coordinates that are nearest neighbors for each location. Recall that the order of the coordinates matters – so, for coordinate $i = 1, \dots, N$, `determineNeighbors` finds the k nearest coordinates (in terms of Euclidean distance) from the preceding $i - 1$ coordinates. A necessary implication of this is that the first coordinate has no neighbors and coordinates $i = 2, \dots, k$ only have $i - 1$ neighbors. The wrapper `sgvSetup` function conducts three operations that are required for the SGV likelihood: the re-ordering and neighbor identification already described, as well as a determination of the conditioning sets. Recall from Section 4 that for location $i = 1, \dots, N$, we require the conditioning set $q(i)$ – i.e., for each neighbor j , whether we should condition on $y(\mathbf{s}_j)$ or $z(\mathbf{s}_j)$.

5.2 `nsgpPredict`: posterior prediction

As described in Sections 2 and 4, posterior prediction can be implemented as a straightforward post-processing step for any of the likelihood methods. This functionality is provided in the `nsgpPredict` function, which takes posterior samples generated using a `nsgpModel` object and the `nimble` package.

```
nsgpPredict( model, samples, coords.predict, predict.process = TRUE,
  constants, seed = 0, ... )
```

Here, `model` is a compiled `nimbleModel` (the output of `nsgpModel`), `samples` are the post burn-in MCMC samples, `coords.predict` is a $M \times d$ matrix of the coordinates of the desired prediction locations, `predict.process` determines whether the prediction corresponds to the $y(\cdot)$ process (TRUE) or $z(\cdot)$ (FALSE; this would likely only be used for, e.g., cross-validation). Next, `constants` is an optional list of constants to use for prediction; alternatively, additional arguments can be passed to the function via the `...` argument (as described in Section 5.1; more on this in the next paragraph). Finally, `seed` is an optional random seed argument for reproducibility.

For every parameter process model (other than the spatially constant models), `nsgpPredict` requires corresponding constants for the prediction locations. These prediction constants are similar to the constants needed for the observed locations: generally, the required argument for prediction location corresponds to the required constant for model fitting but with a `P` appended at the beginning. For example, `tau_model = "logLinReg"` requires both `X_tau` (the design matrix for the log-linear regression model for the $\tau(\cdot)$ process) and `PX_tau` (the corresponding quantity for the prediction locations). However, there are a few exceptions; see Tables B.2, B.3, B.4, B.7, B.6, and B.9 in Appendix B for the full list.

When the necessary constants are provided, `nsgpPredict` proceeds to conduct posterior prediction as described in Sections 2 and 4, depending on the likelihood model. The output of the function is a list with two elements: `obs`, a matrix of J posterior predictive samples for the N observed locations (only for `likelihood = "SGV"`, which produces predictions for the observed locations by default; this element is NULL otherwise); and `pred`, a corresponding matrix of posterior predictive samples for the prediction locations. Ordering and neighbor selection for the prediction coordinates in the NNGP and SGV likelihoods are conducted internally, as with `nsgpModel`.

Returning to our example from Section 5.1, using `samples`, the matrix of posterior samples generated from the MCMC, prediction can proceed as follows. Note that we require prediction locations (defined on a grid), as well as corresponding design matrices:

```
R> M <- 20^2
R> predCoords <- as.matrix(expand.grid(seq(0,1,length = sqrt(M)),
+   seq(0,1,length = sqrt(M))))
R> Xmat1_pred <- cbind(rep(1,M), predCoords[,1])
R> Xmat2_pred <- cbind(rep(1,M), predCoords[,2])
R> pred_constants <- list( PX_sigma = Xmat1_pred, PX_Sigma = Xmat2_pred,
+   PX_mu = Xmat1_pred )
R> pred <- nsgpPredict(model = Rmodel, samples = samples,
+   coords.predict = predCoords, constants = pred_constants)
```

6 Applications

6.1 Annual precipitation for Colorado in 1981

First, we reproduce an analysis of the precipitation data set used by [Paciorek and Schervish \(2006\)](#) from Colorado, a state in the western United States of America. The data used here consist of monthly precipitation recorded at each of approximately 400 weather stations in Colorado; we specifically analyze annual precipitation from 1981, as this year has the most stations ($N = 217$) without missing monthly values. Annual precipitation totals are given in millimeters, and we analyze the log of total precipitation to make the Gaussian process assumption more appropriate (see Figure 1). Figure 1 also shows the diverse topography in Colorado (panel c) as well as a derived measure of the change in elevation (“slope”; panel d), measured as a west-to-east gradient. The specific analysis is an illustration of two previous analyses of this data set: (1) the original analysis in [Paciorek and Schervish \(2006\)](#), and (2) a subsequent analysis using the regression-based nonstationary covariance function from [Risser and Calder \(2015\)](#). Our goal is to demonstrate how these models, both of which use the exact GP likelihood, can be quickly implemented using the **BayesNSGP** package and **nimble**.

For each of the following analyses, we first load the data and calculate the necessary constants. Note that the design matrix for replicating the analysis of [Risser and Calder \(2015\)](#) (`Xmat`) uses a standardized version of elevation and slope.

```
R> # Load raw data
R> COprecip <- read.csv("data/COprecip1981.csv")
R> # Various constants and distance matrices
R> coords <- as.matrix(COprecip[,c("Longitude", "Latitude")])
R> data <- COprecip$logPrecip
R> N <- nrow(coords)
R> Xmat <- unname(lm(logPrecip ~ Zelevation*Zslope10, x = TRUE,
+   data = COprecip)$x)
```

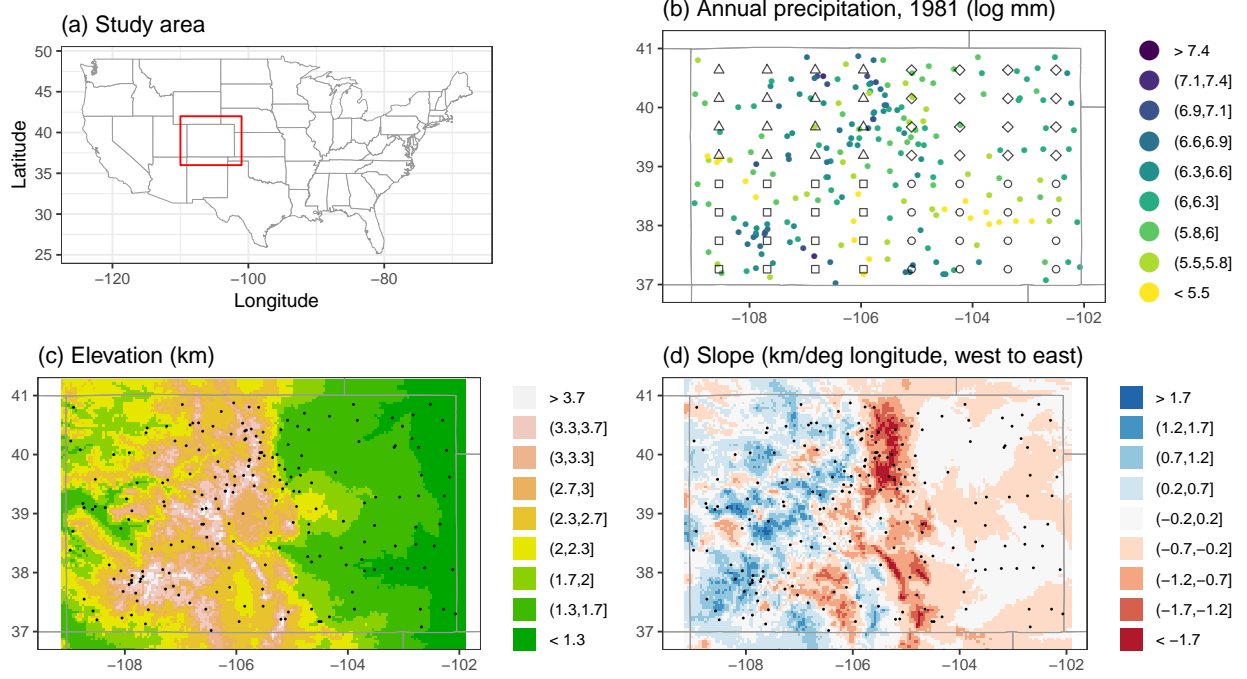


Figure 1: The area of study (panel a), with annual precipitation totals for weather stations in 1981 (panel b, in log mm). Elevation (km) and west-to-east gradient (km per °longitude) shown in panels (c) and (d), with the weather station locations overlaid. Panel (b) also includes the knot locations, where the shape of the plotted point indicates the four sub-blocks used to sample the high-dimensional latent processes for $\Sigma(\cdot)$.

6.1.1 Original analysis

In [Paciorek and Schervish \(2006\)](#), each of the mean $\mu(\mathbf{s})$, the nugget variance $\tau(\mathbf{s})$, and the spatial variance $\sigma(\mathbf{s})$ were modeled as unknown constants, while the anisotropy process $\Sigma(\mathbf{s})$ was modeled using an approximation to a Gaussian process. The following aspects of the analysis are designed to match [Paciorek and Schervish \(2006\)](#):

- Use a coarse, evenly spaced 8×8 grid of $K = 64$ knot locations.
- Fix the smoothness of the latent GPs to be $\nu_\phi = 5$ (below, this is `Sigma_HP2`).
- [Paciorek and Schervish \(2006\)](#) assign a uniform prior on the log scale to the latent GP range, with upper bound $\log 3.85$ and lower bound $\log 0.1$; instead, we use a $U(0, 3.85)$ prior on this parameter (below, the upper bound is `Sigma_HP3`).
- In the original paper they estimate the data-level smoothness with a $U(0.5, 30)$ prior while we fix this smoothness parameter at $\nu = 2$ (below this is `nu = 2`).
- We set an upper bound on the eigenvalue processes to be 16 (below, this is `max-AnisoDist = 16`).

Note that unlike [Paciorek and Schervish \(2006\)](#) we estimate the mean and standard deviation of the latent GPs (i.e., μ_ϕ and σ_ϕ): the GP means are assigned Gaussian priors with zero mean and standard deviation `Sigma_HP1` (the first is for the two eigenvalue processes and the second is for the rotation process); the GP standard deviations are assigned uniform priors over the interval from zero to `Sigma_HP4` (again, the first is for the two eigenvalue processes and the second is for the rotation process). Finally, the spatial mean is assigned a Gaussian prior with mean zero and standard deviation `mu_HP1`.

Denote `coords` to be the $N \times 2$ matrix of longitude and latitude for each of the station locations; the model can be set up as follows:

```
R> # Set up the knot locations
R> x_min <- min(coords[,1]); x_max <- max(coords[,1])
R> y_min <- min(coords[,2]); y_max <- max(coords[,2])
R> knot_coords <- expand.grid(
+   lon = seq(from = x_min + 0.5*(x_max - x_min)/8,
+   to = x_max - 0.5*(x_max - x_min)/8, length = 8),
+   lat = seq(from = y_min + 0.5*(y_max - y_min)/8,
+   to = y_max - 0.5*(y_max - y_min)/8, length = 8) )
R> # Constants for the Paciorek/Schervish analysis
R> constants_PacScher <- list( nu = 2, mu_HP1 = 10,
+   Sigma_knot_coords = knot_coords, Sigma_HP1 = c(10,10),
+   Sigma_HP2 = rep(5,2), Sigma_HP3 = rep(3.85,2),
+   Sigma_HP4 = c(10,20), maxAnisoDist = 16 )
```

The nimble model can be created and configured using

```
R> Rmodel <- nsgpModel( likelihood = "fullGP", coords = coords, data = data,
+   constants = constants_PacScher, Sigma_model = "npApproxGP")
R> conf <- configureMCMC(Rmodel)
```

Note that here `nsgpModel()` uses defaults of `tau_model = "constant"`, `sigma_model = "constant"`, and `mu_model = "constant"`. As before, we can query the default samplers for this model:

```
R> conf$printSamplers()
[1] RW sampler: alpha
[2] RW sampler: delta
[3] RW sampler: SigmaGP_mu[1]
[4] RW sampler: SigmaGP_mu[2]
[5] RW sampler: SigmaGP_phi[1]
[6] RW sampler: SigmaGP_phi[2]
[7] RW sampler: SigmaGP_sigma[1]
[8] RW sampler: SigmaGP_sigma[2]
[9] RW sampler: beta
[10] RW_block sampler: w1_Sigma[1:64]
[11] RW_block sampler: w2_Sigma[1:64]
[12] RW_block sampler: w3_Sigma[1:64]
```


from which we can see that the default is univariate random walk samplers for all hyperparameters and a large block sampler for the latent anisotropy processes `w1_Sigma`, `w2_Sigma`, and `w3_Sigma`. As before, a large block sampler for these parameters is likely to be inefficient; instead, we split sampling of these 64 parameters into four blocks of 16, as shown in Figure 1b, as follows:

```
R> knot_groups <- matrix(c(1:4,9:12,17:20,25:28,5:8,13:16,21:24,29:32,
+   32+c(1:4,9:12,17:20,25:28), 32+c(5:8,13:16,21:24,29:32)), ncol = 4)
R> conf$removeSamplers("w1_Sigma[1:64]")
R> conf$removeSamplers("w2_Sigma[1:64]")
R> conf$removeSamplers("w3_Sigma[1:64]")
R> for(h in 1:ncol(knot_groups)){
+   conf$addSampler(target = c(paste0("w1_Sigma[,",knot_groups[,h],"]")),
+   type = "RW_block" )
+   conf$addSampler(target = c(paste0("w2_Sigma[,",knot_groups[,h],"]")),
+   type = "RW_block" )
+   conf$addSampler(target = c(paste0("w3_Sigma[,",knot_groups[,h],"]")),
+   type = "RW_block" )
+ }
```

Next, we can compile the model and build the MCMC:

```
R> Rmcmc <- buildMCMC(conf) # Build the MCMC
R> Cmodel <- compileNimble(Rmodel) # Compile the model
R> Cmcmc <- compileNimble(Rmcmc, project = Rmodel) # Compile the MCMC
```

and then run a total of 50000 iterations of the MCMC (discarding the first 30000 as burn-in):

```
R> samples_PacScher <- runMCMC(Cmcmc, niter = 50000, nburnin = 30000)
```

Finally, posterior prediction for this model (using a thinned chain of posterior samples) proceeds as follows:

```
R> pred_PacScher <- nsgpPredict( model = Rmodel, coords.predict = predCoords
+   samples = samples_PacScher[seq(5,20000,5),] )
```

6.1.2 Subsequent analysis

Using the regression-based analysis of [Risser and Calder \(2015\)](#), covariate information can be included in three parts of the nonstationary model: the mean function, the spatial variance function, and the kernel matrix function. [Risser and Calder \(2015\)](#) consider elevation as well as a covariate that describes change in elevation (“slope”; see Figure 1). Here, we reproduce their FNS-M2 implementation, which includes the main effects of elevation and slope as well as their interaction in each of the mean, variance, and kernel matrix functions. As mentioned above, following [Risser and Calder \(2015\)](#), elevation and slope measurements are standardized in order to put the coefficient estimates on a similar scale.

Setting up the model for this implementation proceeds as follows:


```
R> constants_RisserCalder <- list( nu = 0.5, X_mu = Xmat, mu_HP1 = 10,
+   X_sigma = Xmat, log_sigma_HP1 = 10, X_Sigma = Xmat,
+   Sigma_HP1 = c(10,10), Sigma_HP2 = c(2,2), maxAnisoDist = 16 )
```

Here, we use the exponential correlation (via $\nu = 0.5$) as in [Risser and Calder \(2015\)](#); X_{μ} , X_{σ} , and X_{Σ} are the design matrices for the corresponding parameter processes; the hyperparameters are the mean regression coefficients prior standard deviation (μ_{HP1}), the log spatial standard deviation regression coefficients prior standard deviation (\log_sigma_HP1), the covariance regression coefficients prior standard deviations (Σ_{HP1} ; the first element for the first row of Γ and the second for the second row of Γ), and the upper bound on the uniform priors for ψ_{11} and ψ_{22} (Σ_{HP2}). Finally, to match the [Paciorek and Schervish \(2006\)](#) analysis, we restrict the diagonal elements to lie in $(0, 16)$ (this is `maxAnisoDist = 16`).

Compiling the model, updating the samplers, and building the MCMC proceeds as before:

```
R> Rmodel <- nsgpModel( likelihood = "fullGP",
+   constants = constants_RisserCalder, coords = coords, data = data,
+   mu_model = "linReg", sigma_model = "logLinReg", Sigma_model = "covReg" )
R> conf <- configureMCMC(Rmodel)
R> conf$removeSamplers( c("psi11", "psi22", "rho") )
R> conf$addSampler( target = c("psi11", "psi22", "rho"), type = "RW_block" )
R> Rmcmc <- buildMCMC(conf) # Build the MCMC
R> Cmodel <- compileNimble(Rmodel) # Compile the model
R> Cmcmc <- compileNimble(Rmcmc, project = Rmodel) # Compile the MCMC
```

Note that we again use the default `tau_model = "constant"` and furthermore have implemented adaptive random walk samplers for all parameters, except for a block Metropolis Hastings sampler for the parameters in Ψ . Again, a total of 30000 iterations of the MCMC (discarding the first 10000 as burn-in) proceeds as follows:

```
R> samples_RisserCalder <- runMCMC(Cmcmc, niter = 30000, nburnin = 10000)
```

Finally, similar to the previous analysis, posterior prediction for this model can be conducted as follows (using a thinned chain of posterior samples):

```
R> pred_RisserCalder <- nsgpPredict(model = Rmodel,
+   samples = samples_RisserCalder[seq(5,20000,5),],
+   coords.predict = predCoords, PX_sigma = Xmat_pred,
+   PX_Sigma = Xmat_pred, PX_mu = Xmat_pred )
```

6.1.3 Results

In spite of the MCMC for the [Paciorek and Schervish \(2006\)](#) analysis being notoriously difficult to run, the sub-block random walk samplers are effective at sampling the highly correlated, high-dimensional posteriors for each of $\{w_1(\cdot), w_2(\cdot), w_3(\cdot)\}$. The MCMC for both models actually converges somewhat quickly (well within 30,000 iterations); the computational time for running the MCMC and prediction (not including the time for **nimble**

Table 1: Computational time for the Markov chain Monte Carlo (MCMC; minutes per 1,000 samples) and drawing posterior samples (minutes per 100 samples) for each of the analyses in Section 6.1. Computing times are given in minutes; all times correspond to running the analysis on one core of a 32-core (AMD Opteron Processor 8384) machine with 256 GB memory.

Statistical model	MCMC time	Prediction time
Paciorek and Schervish (2006)	29.4	6.6
Risser and Calder (2015)	9.0	4.1

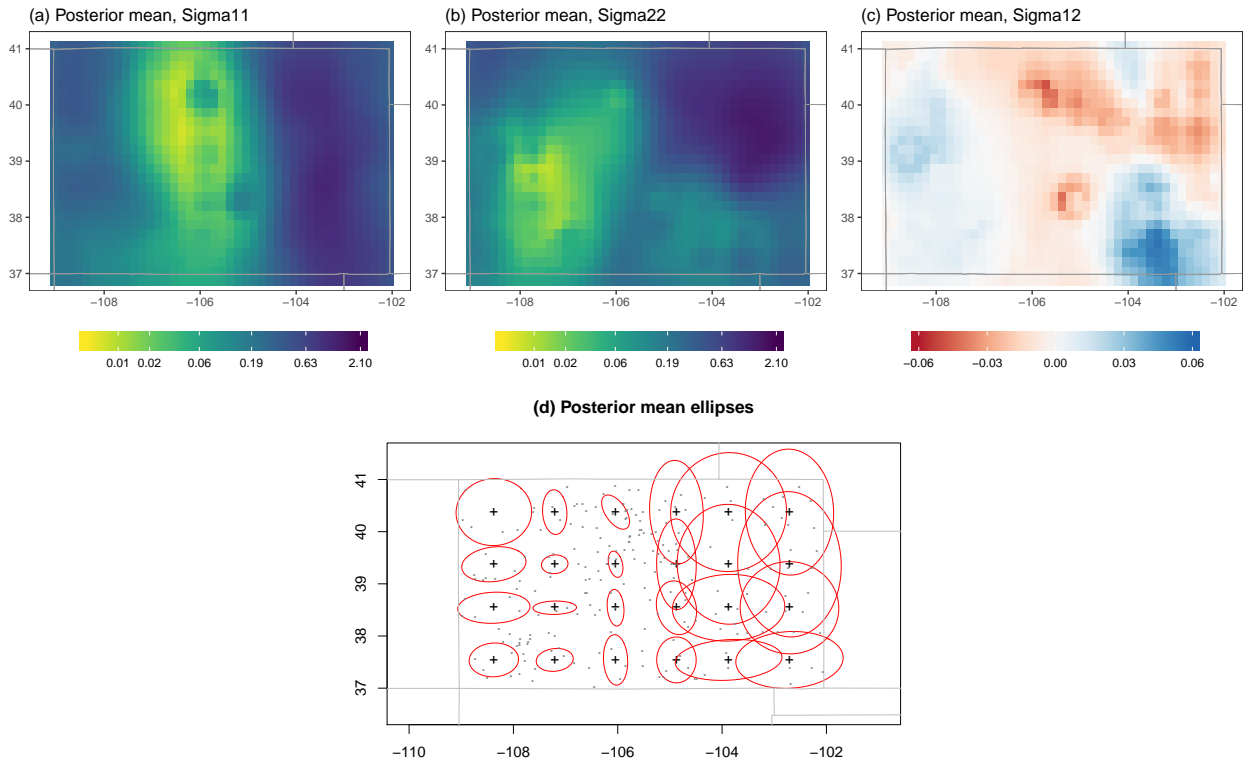


Figure 2: Panels (a), (b), and (c) contain spatial maps of the posterior mean of the anisotropy process $\Sigma(\cdot)$ elements (namely $\Sigma_{11}(\cdot)$, $\Sigma_{22}(\cdot)$, and $\Sigma_{12}(\cdot)$, respectively). To simultaneously view the effect of these parameter processes, panel (d) shows the posterior mean 50% probability ellipse of a bivariate Gaussian density with covariance matrix $\Sigma(\cdot)$ for a set of representative locations over the domain (compare with Figure 4d in (Paciorek and Schervish, 2006)). Note that these ellipses are only meant to provide a qualitative summary of the direction and magnitude of spatial dependence over the domain.

compilation) is shown in Table 1. The MCMC for both models can be run on the order of hours (although the Paciorek and Schervish analysis is much slower), which is significantly faster than (at least) the analysis in Risser and Calder (2015), which the authors mention

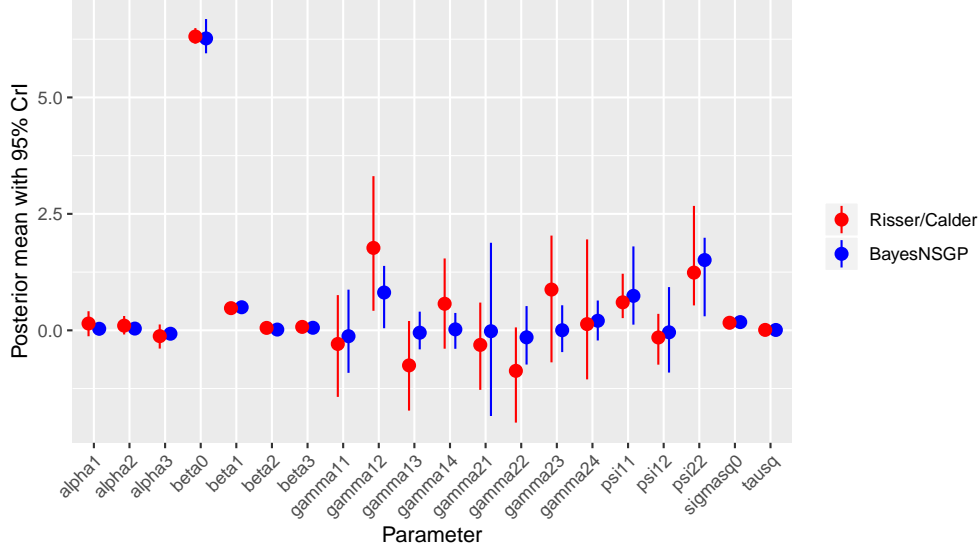


Figure 3: Posterior mean and 95% credible intervals for all statistical parameters in the covariance regression analysis of [Risser and Calder \(2015\)](#), comparing the original analysis as well as the **BayesNSGP** analysis provided in this paper.

took approximately 20 hours for 10,000 iterations (although [Risser and Calder, 2015](#), note that their algorithm is not as efficient as it could be, and regardless the compute machines are not comparable).

While not explicitly provided in [Paciorek and Schervish \(2006\)](#), posterior means (standard deviations) of the spatially-constant mean μ , spatial variance σ^2 , and nugget variance τ^2 are, respectively, 6.172 (0.091), 0.221 (0.042), and 0.013 (0.004) – note, however, that the posterior means are close to the maximum likelihood estimates for the stationary Gaussian process provided in Table 1 of [Paciorek and Schervish \(2006\)](#). The anisotropy process $\Sigma(\cdot)$ is somewhat more difficult to summarize, given the high dimensionality of the parameters involved; however, spatial maps of the elements of $\Sigma(\cdot)$ are shown in Figure 2(a)-(c), with a qualitative summary of the spatially-varying magnitude and direction of spatial dependence in Figure 2(d). The ellipses in panel (d) represent the posterior mean 50% probability ellipse of a bivariate Gaussian density with covariance matrix $\Sigma(\cdot)$ for a set of representative locations over the domain. This figure is comparable to Figure 4d [Paciorek and Schervish \(2006\)](#): note that as in the original analysis, the ellipses (and hence range of dependence) are much smaller in the center of the domain—where there is highly diverse topography—but large in the eastern part of Colorado where the topography is flat, and also somewhat larger in the far western part of the state where the topography is much less heterogeneous.

Next, we can compare posterior summaries for all statistical parameters in the covariance regression analysis of [Risser and Calder \(2015\)](#); specifically, comparing the posterior means and 95% credible intervals taken from Table 1 of [Risser and Calder \(2015\)](#) with the results obtained from our analysis using **BayesNSGP**. This comparison is provided in Figure 3: clearly, the **BayesNSGP** analysis reproduces the results from the original analysis.

Finally, we provide posterior prediction maps (both the mean and standard deviation)

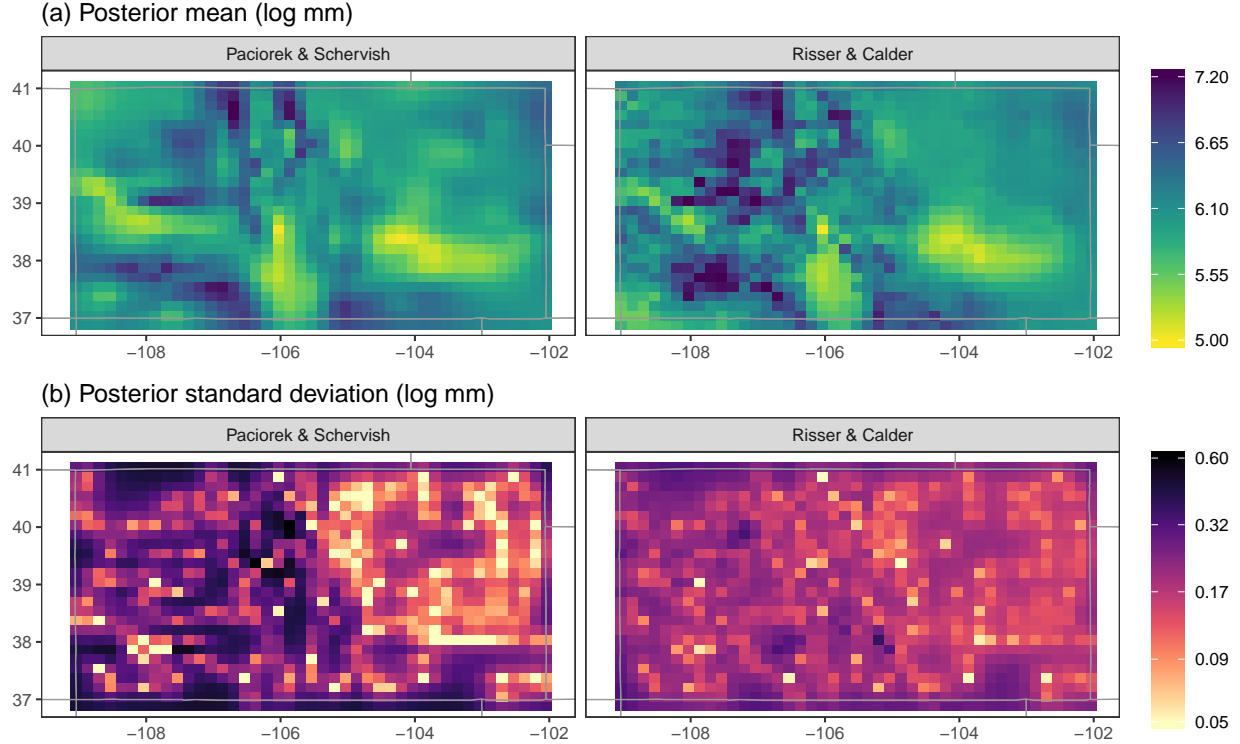


Figure 4: Posterior mean and standard deviation (log mm) of the posterior predictive samples for both statistical models.

for both analyses in Figure 4 (these plots are not provided for [Risser and Calder, 2015](#); the two left panels can be compared with Figure 3 in [Paciorek and Schervish, 2006](#)). The two analyses using **BayesNSGP** yield similar posterior mean prediction maps, although the map for [Risser and Calder \(2015\)](#) is much less smooth than [Paciorek and Schervish \(2006\)](#) (likely a function of both using the exponential instead of the Matérn as well as including topographic covariates in the mean). Furthermore, the standard errors for the [Paciorek and Schervish \(2006\)](#) model are almost uniformly larger, particularly in the western part of the domain.

In summary, in this section we have demonstrated how the **BayesNSGP** package can quickly and efficiently reproduce the results of two separate analyses of the same data set using a nonstationary covariance function with an exact Gaussian process likelihood.

6.2 Total precipitation over CONUS

Next, we analyze a larger data set consisting of measurements of the log daily precipitation rate from the Global Historical Climatology Network-Daily database (GHCN-D; [Menne et al., 2012a,b](#)) over the contiguous United States (CONUS) for the 2018 water year (October 1, 2017 to September 30, 2018). A total of 2311 GHCN-D stations (out of 21,269 total; see Figure 5) have no missing daily values over this time period; we furthermore limit the analysis to the $N = 1470$ stations to the west of the 90°W meridian, as daily precipitation rates

are relatively much smoother in the eastern part of CONUS. Specifically, we are interested in analyzing the average daily precipitation over this water year (shown in Figure 5a along with the study area), modeled on the log scale. In this analysis we will compare the exact Gaussian process likelihood (`likelihood = "fullGP"`) with the sparse general Vecchia likelihood (`likelihood = "SGV"`), since the size of this data set is still reasonable for fitting a Bayesian model using the exact likelihood.

For this analysis, we allow the mean, spatial variance, and anisotropy process to vary across CONUS while fixing the nugget variance to be a constant. There is a clear relationship between elevation and precipitation rate, particularly in the west, although this relationship is different in, e.g., Colorado (where higher elevations are dryer) compared with the Sierra Nevada (where higher elevations are wetter) – so, we model the mean as varying linearly with elevation interacted with the x -coordinate. In order to allow the signal-to-noise ratio to vary smoothly over the domain, we use the approximate latent GP model for the spatial variance process. Finally, from the previous application, we expect the direction and magnitude of spatial dependence to depend on elevation, so we model the three anisotropy components as varying linearly with elevation (using the componentwise regression approach). The statistical model described here can be set up as follows: first loading the data

```
R> CONUSprecip <- read.csv("data/CONUS_WY2018.csv")
R> CONUSprecip <- CONUSprecip[CONUSprecip$longitude < -98,]
R> coords <- as.matrix(CONUSprecip[,c("longitude", "latitude")])
R> data <- CONUSprecip$logPR
R> CONUSprecip$zelevation <- scale(CONUSprecip$xelevation)
R> CONUSprecip$zlongitude <- scale(longitude)
R> Xmat1 <- unname(lm(logPR ~ Zelevation, x = TRUE, data = CONUSprecip)$x)
R> Xmat2 <- unname(lm(logPR ~ Zelevation*Zlongitude, x = TRUE,
+   data = CONUSprecip)$x)
```

(note that we again standardize the mean and anisotropy covariates) and setting up the knot locations (48 total) as

```
R> x_min <- min(CONUSprecip[, "longitude"])
R> x_max <- max(CONUSprecip[, "longitude"])
R> y_min <- min(CONUSprecip[, "latitude"])
R> y_max <- max(CONUSprecip[, "latitude"])
R> knot_coords <- expand.grid(
+   lon = seq(from = x_min - 0.25, to = x_max + 0.25, length = 9),
+   lat = seq(from = y_min - 0.75, to = y_max, length = 6) )
R> knot_coords <- as.matrix(knot_coords)
R> knot_coords <- knot_coords[-c(1:5, 10),]
```

(several of the knot locations are removed due to the irregular shape of western CONUS) we can then set up the constants and model:

```
R> constants <- list( nu = 0.5, k = 15, tau_HP1 = 10,
+   sigma_knot_coords = knot_coords, sigma_HP1 = 10, sigma_HP2 = 5,
```

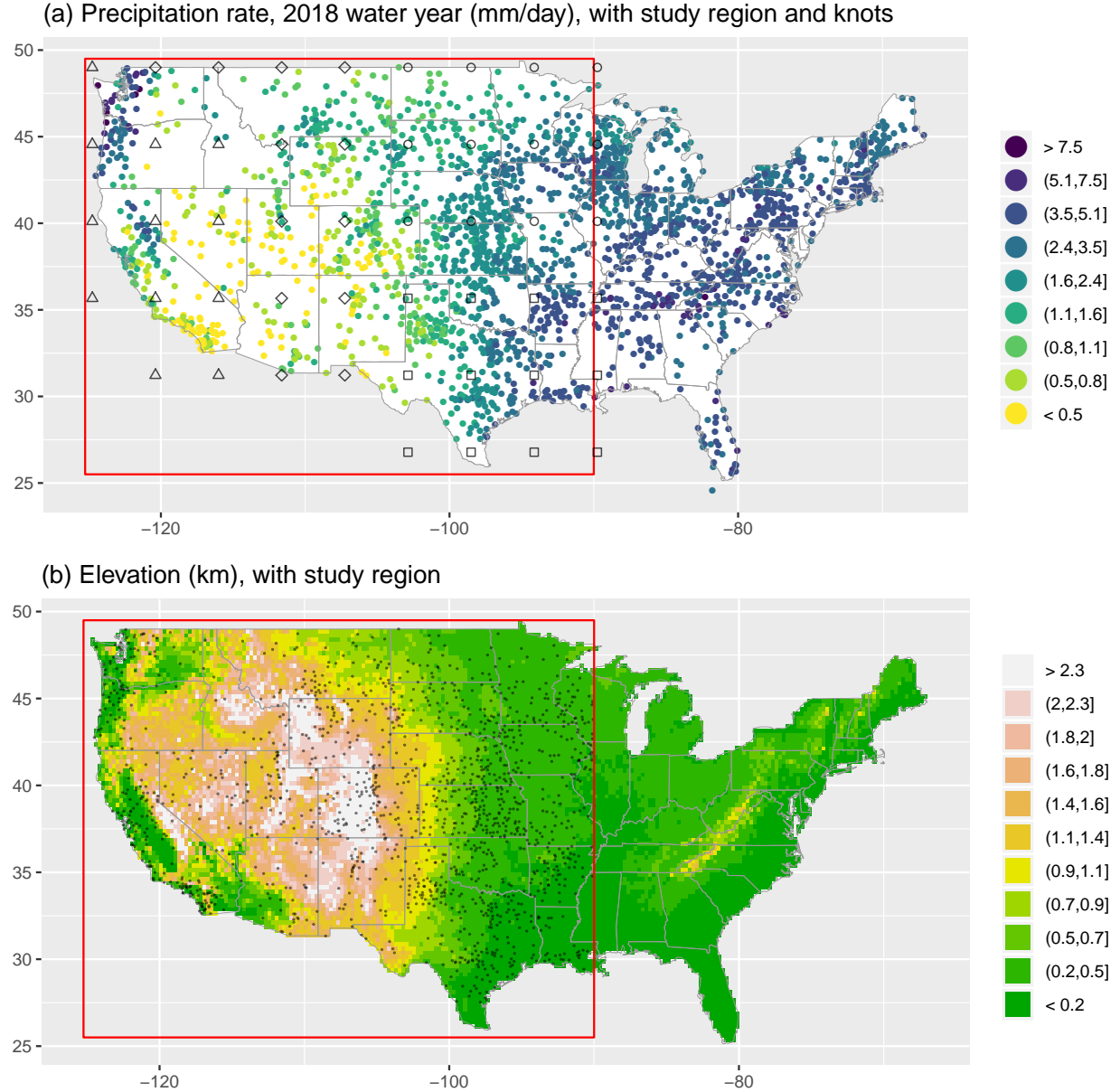


Figure 5: Precipitation rate during the 2018 water year (October 1, 2017 to September 30, 2018) for the 2311 GHCN stations with no missing daily measurements over this time period (mm day^{-1} ; panel a), and elevation (km; panel b) with the station locations overlaid. For this analysis, we consider the $N = 1470$ weather stations in western CONUS, where precipitation rates are much more heterogeneous than in the eastern CONUS. Panel (a) also shows the knot locations, where the shape represents the sampling sub-block.

```
+ sigma_HP3 = 10, sigma_HP4 = 10, X_Sigma = Xmat1, Sigma_HP1 = 5,
+ maxAnisoDist = max(dist(coords)), X_mu = Xmat2, mu_HP1 = 10 )
R> Rmodel <- nsgpModel( likelihood = "fullGP", constants = constants,
+ coords = coords, data = data, tau_model = "constant",
```

```
+ sigma_model = "approxGP", mu_model = "linReg", Sigma_model = "compReg")
```

Note that here we use the exact GP likelihood (`likelihood = "fullGP"`), although the same code can be used for SGV by simply changing this to `likelihood = "SGV"`.

Given the high-dimensional parameter space, we can utilize the block multivariate samplers provided with the **nimble** package. First, we configure the model and block together the mean and anisotropy process parameters as well as the latent GP hyperparameters:

```
R> conf <- configureMCMC(Rmodel)
R> conf$removeSamplers(c("beta[1]", "beta[2]", "beta[3]", "beta[4]"))
R> conf$removeSamplers(c("Sigma_coef1[1]", "Sigma_coef1[2]",
+   "Sigma_coef2[1]", "Sigma_coef2[2]",
+   "Sigma_coef3[1]", "Sigma_coef3[2]"))
R> conf$removeSamplers(c("sigmaGP_mu", "sigmaGP_phi", "sigmaGP_sigma"))
R> conf$addSampler(target = c("beta[1]", "beta[2]", "beta[3]", "beta[4]"),
+   type = "RW_block")
R> conf$addSampler(target = c("Sigma_coef1[1]", "Sigma_coef1[2]",
+   "Sigma_coef2[1]", "Sigma_coef2[2]", "Sigma_coef3[1]",
+   "Sigma_coef3[2]"), type = "RW_block")
R> conf$addSampler(target = c("sigmaGP_mu", "sigmaGP_phi", "sigmaGP_sigma"),
+   type = "RW_block")
```

As with the previous example, we opt to break up sampling of the latent GP effects for the $\sigma(\cdot)$ process into four sub-blocks of 12 parameters each. The location of the knots and their sampling groups are shown in Figure 5(a). These samplers can be set up as

```
R> knot_groups <- matrix(c(1:4, 9:12, 18:21,
+   27:30, 36:39, 45:48,
+   5:6, 13:15, 22:24, 31:33, 40:42,
+   7:8, 16:17, 25:26, 34:35, 43:44), ncol = 4)
R> conf$removeSamplers("w_sigma[1:48]")
R> for(h in 1:ncol(knot_groups)){
+   conf$addSampler(target = c(paste0("w_sigma[", knot_groups[,h], "]")),
+   type = "RW_block" )
+ }
```

Finally, we can check to confirm that the samplers have been set up as intended:

```
R> conf$printSamplers()
[1] RW sampler: delta
[2] RW_block sampler: beta[1], beta[2], beta[3], beta[4]
[3] RW_block sampler: Sigma_coef1[1], Sigma_coef1[2], Sigma_coef2[1], ...
[4] RW_block sampler: sigmaGP_mu, sigmaGP_phi, sigmaGP_sigma
[5] RW_block sampler: w_sigma[1], w_sigma[2], w_sigma[3], w_sigma[4], ...
[6] RW_block sampler: w_sigma[27], w_sigma[28], w_sigma[29], w_sigma[30], ...
[7] RW_block sampler: w_sigma[5], w_sigma[6], w_sigma[13], w_sigma[14], ...
[8] RW_block sampler: w_sigma[41], w_sigma[42], w_sigma[7], w_sigma[8], ...
```


Table 2: Computational time for the Markov chain Monte Carlo (MCMC; minutes per 1,000 samples) and drawing posterior samples (minutes per sample) for each likelihood method in Section 6.2. Computing times are given in minutes; all times correspond to running the analysis on one core of a 32-core (AMD Opteron Processor 8384) machine with 256 GB memory.

Likelihood	MCMC time	Prediction time
Exact GP	564.7	14.5
SGV	48.5	0.4

(again, the `w_sigma` and `Sigma_coef` samplers have been truncated).

With our model object fully customized (for both the exact likelihood and SGV), we can now build, compile, and run the MCMC for 40,000 iterations (with 30,000 iterations discarded as burn-in) as

```
R> Rmcmc <- buildMCMC(conf) # Build the MCMC
R> Cmodel <- compileNimble(Rmodel) # Compile the model
R> Cmcmc <- compileNimble(Rmcmc, project = Rmodel) # Compile the MCMC
R> samples <- runMCMC(Cmcmc, niter = 40000, nburnin = 30000) # Run
```

And, once the posterior samples have been obtain, we can proceed with posterior prediction (again for either likelihood method) using a thinned chain as follows:

```
R> pred <- nsqpPredict(model = Rmodel,
+   samples = samples[seq(from=2,to=10000,by=2),],
+   coords.predict = predCoords, PX_Sigma = PXmat1, PX_mu = PXmat2)
```

The computational times for running the MCMC and obtaining posterior predictive draws for both likelihood methods are shown in Table 2. Clearly, the SGV likelihood gives a large order of magnitude decrease in the computational time for both tasks, although the performance gain for SGV is enhanced for the prediction. However, the two likelihood methods also yield indistinguishable results for both the posterior distributions of all parameters (see Figure 6) as well as the posterior predictions (see Figure 7).

6.3 Return values for extreme Borel winter surface temperature

Finally, we analyze a much larger data set based on the output of an ensemble of climate model simulations from version 5.1 of the Community Atmospheric Model global atmosphere/land climate model, run in its conventional $\sim 1^\circ$ longitude/latitude configuration (Neale et al., 2012; Stone et al., 2018). These simulations were run under the experiment protocols of the C20C+ Detection and Attribution Project (Stone and Pall, 2016) following two climate scenarios (Angéilil et al., 2017). We utilize simulations from the “factual” (or historical) scenario, which is driven by observed boundary conditions of atmospheric chemistry (greenhouse gases, tropospheric and stratospheric aerosols, ozone), solar luminosity,

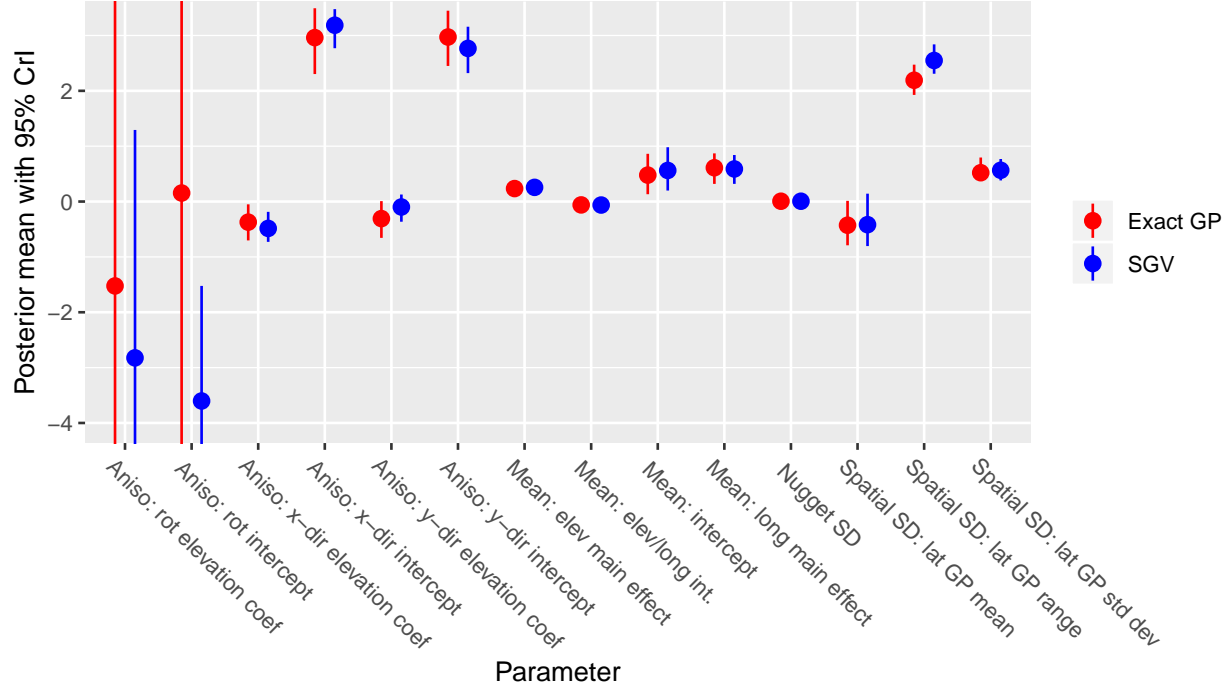


Figure 6: Posterior mean and 95% credible intervals for all statistical parameters (excluding the latent GP effects) in the analysis of total precipitation over the western CONUS, comparing the exact Gaussian process and SGV likelihoods.

land use/cover, and the ocean surface (temperature and ice coverage). The data and further details on the simulations are available at <http://portal.nersc.gov/c20c>; we use the 50-member ensemble that covers 01/1959 to 12/2018. A climate model ensemble is a set of runs from a particular climate model where each ensemble member has the same boundary conditions but stochastically perturbed initial conditions; the different ensemble members can be considered independent samples from the population defined by the climate model.

This large ensemble of simulations is particularly suitable for evaluating climate extremes. As such, here we analyze derived maximum likelihood estimates of 20-year return values for the DJF seasonal mean temperature over 1960-2015. The 20-year return value corresponds to the seasonal mean temperature value that is expected to occur once every 20 years, on average (for more information, we refer the interested reader to [Coles, 2001](#), chapter 3). These return values are calculated as follows: first, using the 50-member ensemble of simulations, for each grid cell we first extract the ensemble maximum DJF average temperature from each year, leaving us with a sample of 56 maxima. Next, we fit a Generalized Extreme Value distribution to these maxima using maximum likelihood estimation (using the **climextRemes** package; [Paciorek, 2016](#)) and calculate the 20-year return value. The default optimization procedure fails for some grid cells, in which case we record a missing value; otherwise, the estimated return values are given in degrees Kelvin (K) and are considered fixed for the remainder of the analysis (see Figure 8; grid cells where the optimization failed are plotted in gray).

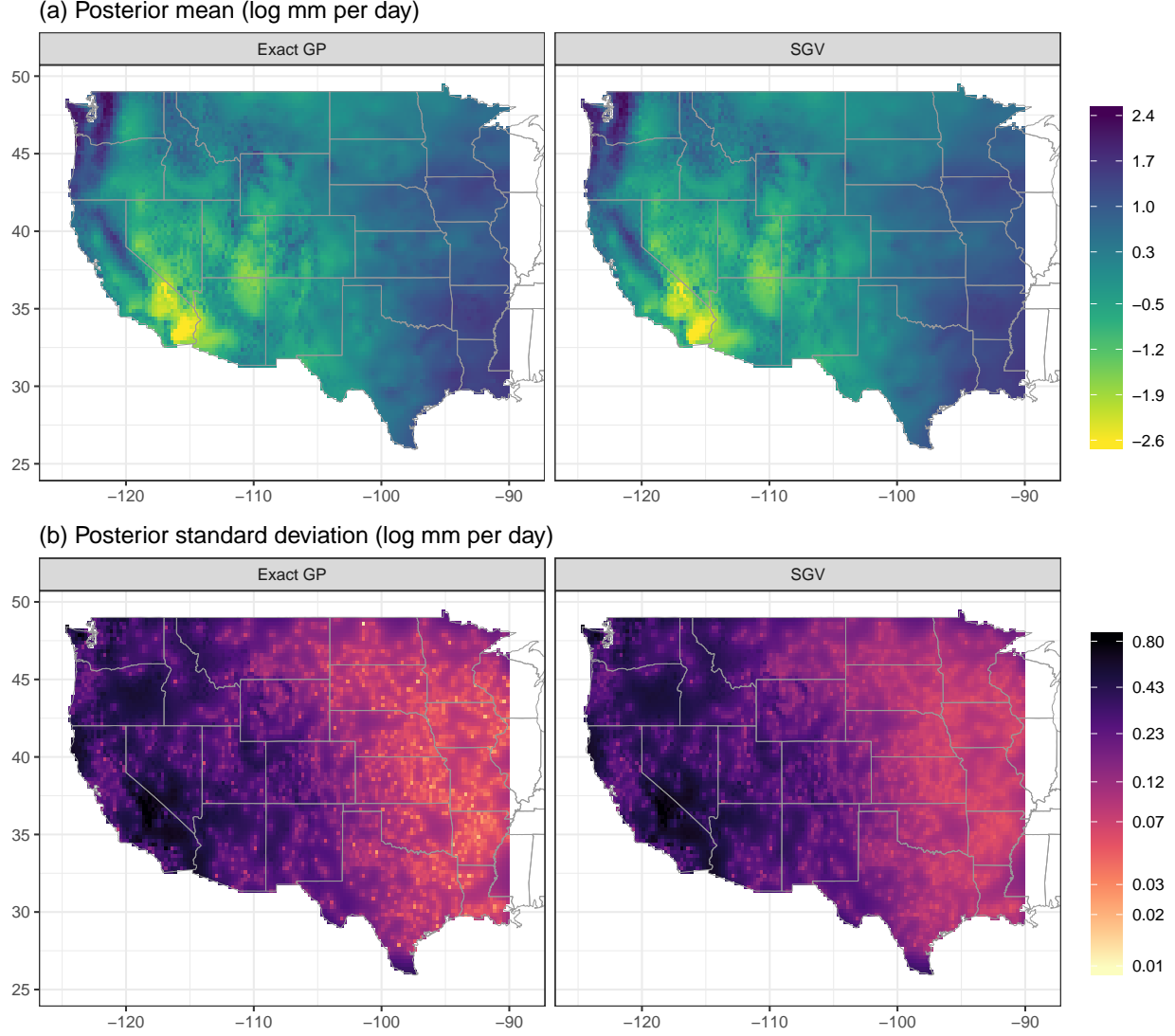


Figure 7: Posterior mean and standard deviation ($\log \text{ mm day}^{-1}$) of the posterior predictive samples for total precipitation over CONUS in the 2018 water year, comparing the exact Gaussian process and SGV likelihoods.

A spatial model fit to these data is useful for several reasons: (1) to estimate return values for the grid cells with missing values, (2) to reduce the signal-to-noise ratio of the return value estimates by borrowing strength over space, (3) to understand how the spatial dependence properties of the return values vary over space, and (4) to emulate the climate model for generating additional spatial fields with corresponding statistical properties (see, e.g., [Li and Sun, 2019](#)). Particularly for the latter two purposes, for a global data set it is important to allow the properties of the covariance function to vary over space. For now focusing on the spatial variance and anisotropy, as a simple way of characterizing these changes we arbitrarily split the spatial domain into six equally sized subregions (divided at the equator and also the 0° and $\pm 120^\circ$ meridians; shown in Figure 8) and assign each subregion a unique spatial vari-

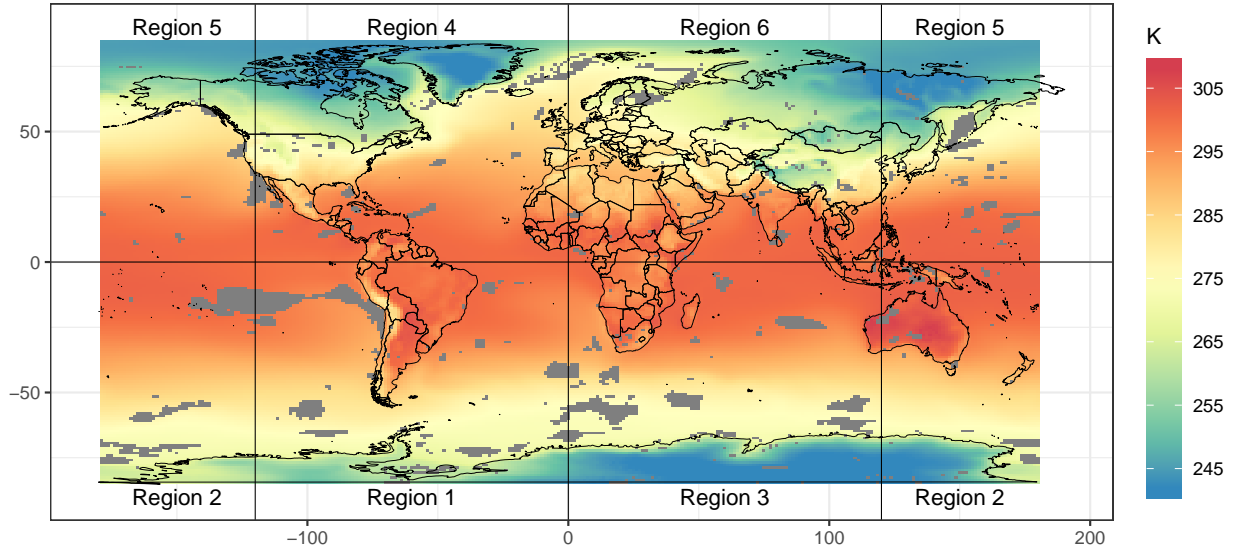


Figure 8: Derived maximum likelihood estimates of the 20-year return value for DJF average temperature at the surface or TAS (in K), calculated independently for each grid cell using the ensemble maximum DJF average temperature in each year from the CAM5.1-1degree simulations over 1960-2015. Gray cells indicate grid cells where the maximum likelihood estimation failed; the numbers correspond to the spatial subregions considered in our analysis.

ance and anisotropy (although these processes are constant within-subregion); denote these parameters as $\{\sigma_r : r = 1, \dots, 6\}$ and $\{\Sigma_r : r = 1, \dots, 6\}$. Note that below these parameters can be estimated using the "logLinReg" and "compRegIso" statistical models by defining an appropriate design matrix based on the region membership. Given that we are dealing with gridded data that are relatively smooth, we simply specify the nugget variance to be an unknown spatial constant. Furthermore, we maintain a constant spatial mean to emphasize the second-order properties of the return values. Finally, since the covariance function here is not valid on the sphere, we instead represent the longitude/latitude coordinates as points in a three-dimensional space and therefore must use the locally isotropic version of the covariance function. The local isotropy is still modeled regionally.

The model is defined on a 288×192 global grid with 55,296 grid cells, although we exclude the extreme pole model grid cells with a latitude of greater than ± 85 leaving 51,840 cells, $N = 49,217$ of which are non-missing. The size of this data set makes it virtually impossible to analyze using the exact Gaussian process likelihood; on the other hand, inference is possible using the approximate GP methods. Here, we apply the NNGP likelihood to this data set.

The statistical model in the previous paragraphs can be implemented in **BayesNSGP** as follows:

```
R> # Load data
```

```

R> tasRV20_DF_all <- read.csv("data/C20C_DJFtasRV20_trend.csv")
R> # Remove pole measurements
R> tasRV20_DF_all <- tasRV20_DF_all[abs(tasRV20_DF_all$latitude) < 85,]
R> # Remove NA's for fitting
R> tasRV20_DF <- tasRV20_DF_all[!is.na(tasRV20_DF_all$rv20),]
R> # Design matrix
R> Xmat <- unname(lm(rv20 ~ region, x = TRUE, data = tasRV20_DF)$x)
R> # Convert lon/lat to x/y/z
R> xyz.crds <- matrix(NA,nrow(tasRV20_DF),3)
R> # Transform degrees to radians
R> lat.radians <- tasRV20_DF$latitude*(pi/180)
R> lon.radians <- tasRV20_DF$longitude*(pi/180)
R> for(i in 1:nrow(xyz.crds)){ # Units = 1000 km. Earth diameter ~ 6371km.
+   xyz.crds[i,1] <- 6.371*cos(lat.radians[i])*cos(lon.radians[i])
+   xyz.crds[i,2] <- 6.371*cos(lat.radians[i])*sin(lon.radians[i])
+   xyz.crds[i,3] <- 6.371*sin(lat.radians[i])
+ }
R> # Setup constants for NNGP
R> constants <- list( nu = 5, k = 15, mu_HP1 = 100, X_sigma = Xmat,
+   sigma_HP1 = 10, X_Sigma = Xmat, Sigma_HP1 = 10, maxAnisoDist = 20 )
R> Set up the nimbleModel
R> Rmodel <- nsgpModel(likelihood = "NNGP", constants = constants,
+   coords = round(xyz.crds, 4), data = tasRV20_DF$rv20,
+   sigma_model = "logLinReg", Sigma_model = "compRegIso")

```

While this model does not contain too many parameters, it is still important to use block sampling to account for the correlated parameter space. As such, we apply block samplers for the spatial variance and isotropy ranges in each hemisphere:

```

R> conf <- configureMCMC(Rmodel)
R> conf$removeSamplers(c("alpha[1:6]", "Sigma_coef1[1:6]"))
R> # Regions 1, 2, and 3 are in the southern hemisphere
R> conf$addSampler(target = c("alpha[1]", "alpha[2]", "alpha[3]",
+   "Sigma_coef1[1]", "Sigma_coef1[2]", "Sigma_coef1[3]"), type = "RW_block")
R> # Regions 4, 5, and 6 are in the northern hemisphere
R> conf$addSampler(target = c("alpha[4]", "alpha[5]", "alpha[6]",
+   "Sigma_coef1[4]", "Sigma_coef1[5]", "Sigma_coef1[6]"), type = "RW_block")

```

Running the MCMC then proceeds as before:

```

R> Rmcmc <- buildMCMC(conf) # Build the MCMC
R> Cmodel <- compileNimble(Rmodel) # Compile the model
R> Cmcmc <- compileNimble(Rmcmc, project = Rmodel) # Compile the MCMC
R> samples <- runMCMC(Cmcmc, niter = 10000, nburnin = 5000) # Run

```

And similarly for prediction:

Table 3: Computational time for building and compiling the `nsgpModel`, running the Markov chain Monte Carlo (MCMC; minutes per 1,000 samples), and drawing posterior samples (minutes per sample) for the NNGP. Computing times are given in minutes; all times correspond to running the analysis on one core of a 32-core (AMD Opteron Processor 8384) machine with 256 GB memory.

Build time	MCMC time	Prediction time
36.7	902.5	11.3

```

R> Xmat_pred <- unname(lm(rnorm(nrow(tasRV20_DF_all)) ~ region, x = TRUE,
+   data = tasRV20_DF_all)$x)
R> # Convert lon/lat to x/y/z
R> xyz.crds <- matrix(NA,nrow(tasRV20_DF_all),3)
R> # Transform degrees to radians
R> lat.radians <- tasRV20_DF_all$latitude*(pi/180)
R> lon.radians <- tasRV20_DF_all$longitude*(pi/180)
R> for(i in 1:nrow(xyz.crds)){ # Units = 1000 km
+   xyz.crds[i,1] <- 6.371*cos(lat.radians[i])*cos(lon.radians[i])
+   xyz.crds[i,2] <- 6.371*cos(lat.radians[i])*sin(lon.radians[i])
+   xyz.crds[i,3] <- 6.371*sin(lat.radians[i])
+ }
R> pred <- nsgpPredict(model = Rmodel,
+   samples = samples[seq(from=5,to=5000,by=5),],
+   coords.predict = round(xyz.crds, 4),
+   constants = list(PX_sigma = Xmat_pred, PX_Sigma = Xmat_pred))

```

Computational times for each component of the model fitting and predictions are shown in Table 3. Note that the amount of time it takes to build and compile the model is somewhat non-trivial for this very large data set (on the order of 30 minutes). Furthermore, even with the NNGP likelihood, the MCMC is still quite slow.

The posterior mean for the overall mean is 285.90K, with a 95% credible interval (CrI) of (285.29, 286.50); similarly, for the overall nugget standard deviation, the posterior mean is 0.050K with a 95% CrI of (0.0491, 0.0515). The posterior means and 95% CrIs for the $\{\sigma_r : r = 1, \dots, 6\}$ and $\{\Sigma_r : r = 1, \dots, 6\}$ are shown in Figure 9. In general, the Northern Hemisphere (NH) regions (4-6) have larger spatial variance and shorter length scales, indicating that the return values have a larger degree of spatial heterogeneity in the NH than in the Southern Hemisphere (SH). There are within-NH differences in the posterior distributions for these parameters, although in general regions 4 and 6 (the regions containing most of North America and most of Europe/Asia, respectively) are more similar than region 5 (which contains the North Pacific). The spatial dependence characteristics of these parameters in the SH are much more consistent, with relatively smaller spatial variability and longer spatial length scales.

Finally, we show the posterior predictive mean and standard deviation (both in K) in

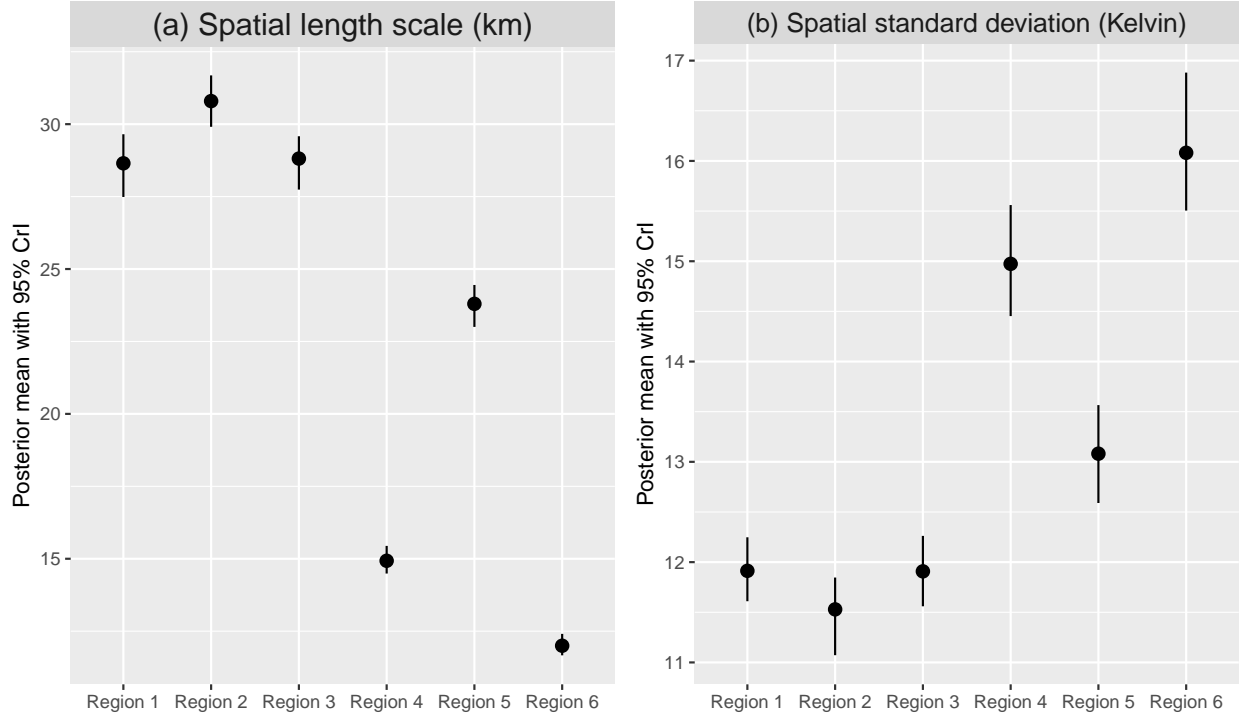


Figure 9: Posterior means and 95% credible intervals (CrI) for the locally isotropic spatial length-scale parameters $\{\Sigma_r : r = 1, \dots, 6\}$ (panel a) and spatial standard deviations $\{\sigma_r : r = 1, \dots, 6\}$; (panel b) for each subregion shown in Figure 8.

Figure 10. Unsurprisingly, given the very small estimated nugget standard deviation ($\approx 0.05K$), the predictive mean looks very similar to the raw data given in Figure 8, with one important difference: the missing values have now been filled in via the local kriging enabled by the NNGP likelihood. Interestingly, the posterior standard deviation is very clearly a function of the proximity to non-missing data values (i.e., the grid cells with a missing data value have much larger uncertainty than those with a non-missing value) but also the spatial subregions: the uncertainty is larger in regions 4 and 6 of the NH relative to the SH. Clearly, the somewhat sharp boundaries in the posterior uncertainty along the subregion borders is unrealistic, but this could be addressed by allowing the spatial dependence parameters to change smoothly over the domain.

7 Discussion

In this paper, we have described the **BayesNSGP** software package for R which provides off-the-shelf functionality for fully Bayesian, nonstationary Gaussian process modeling via a closed-form, convolution-based covariance function with spatially-varying parameters. We furthermore implement approximate Gaussian process inference to account for very large spatial data sets; Bayesian inference and posterior prediction is carried out using Markov chain Monte Carlo methods via the **nimble** package, which enables sampling of the highly

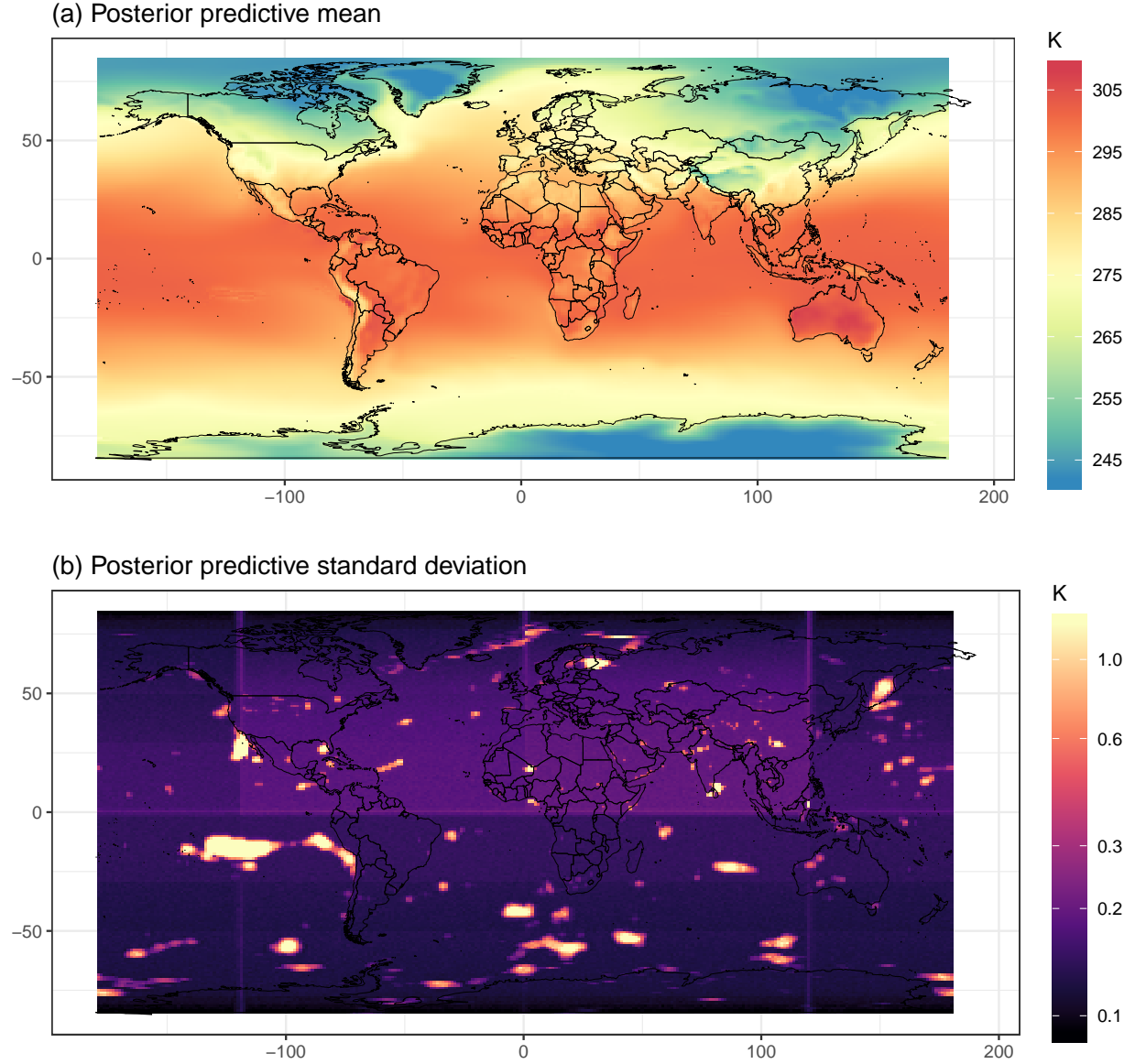


Figure 10: Posterior mean predictions and uncertainty for the 20-year return values shown in Figure 8.

correlated parameter spaces common to nonstationary Gaussian process models. Finally, we demonstrate the features and computational properties of our package using three data sets of varying size, from small (several hundred) to very large (approximately fifty thousand).

As described in Section 4, the approximate Gaussian process methods implemented here (NNGP and SGV) present a trade-off between the quality of the likelihood approximation (SGV is known to provide a better approximation) and the computational speed (NNGP is faster). The fact that NNGP is faster than SGV remains true in our implementation for nonstationary Gaussian processes; as an illustration consider Figure 11, which shows

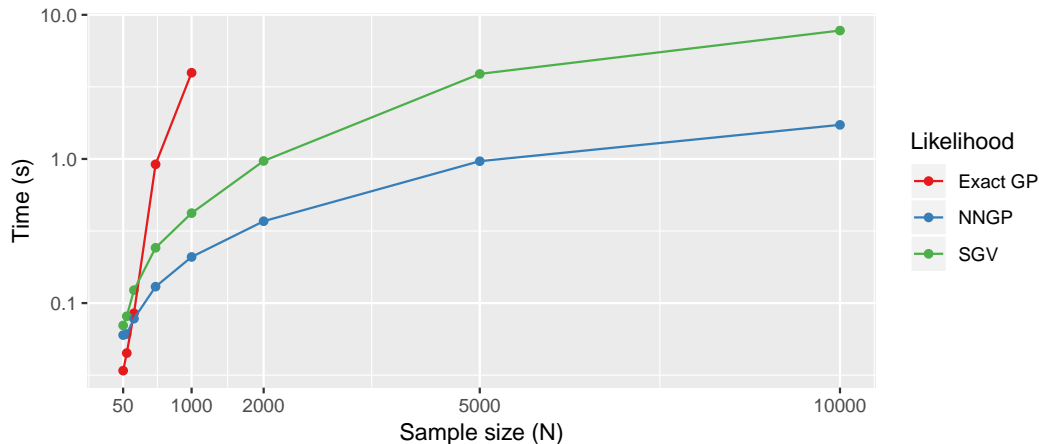


Figure 11: Computational time for a single evaluation of the likelihood for the nonstationary model discussed in Section 5, for each likelihood method and a variety of sample sizes. Times correspond to a 1.6GHz Intel Core i5 machine with 16GB memory.

computational times for a single likelihood evaluation for the toy nonstationary example described in Section 5.1. Note that the exact GP likelihood is actually the fastest for small sample sizes (up to about $N = 200$), while the NNGP is always faster than SGV even for very small data sets; the differences are a significant order of magnitude for $N = 10,000$.

While our methodology enables approximate Gaussian process inference for “very large” data sets, it should be noted that the methodology as implemented here is not extendable to the most modern “massive” data sets with many millions of measurements (Finley et al., 2018 analyze a data set with over 28 million measurements, while Huang et al., 2019 utilize high performance computing to conduct likelihood inference for more than 45 million measurements). For data sets of this size, there are non-negligible memory considerations for loading and manipulating the data; these issues are certainly still a barrier when using the **nimble** functionality. Nonetheless, we argue that our package is still a novel and important contribution to the software for modeling (at least) very large data sets without requiring a customized computing environment or high performance computing: all of the analyses in this paper can be implemented off-the-shelf on a personal laptop.

Acknowledgements

The authors would like to thank Dr. Chris Paciorek for helpful discussion and comments in the development of this software package.

This work was supported by the Regional and Global Model Analysis Program of the Office of Biological and Environmental Research in the Department of Energy Office of Science under contract number DE-AC02-05CH11231. This document was prepared as an account of work sponsored by the United States Government. While this document is believed to contain correct information, neither the United States Government nor any agency thereof, nor the Regents of the University of California, nor any of their employees, makes any war-

ranty, express or implied, or assumes any legal responsibility for the accuracy, completeness, or usefulness of any information, apparatus, product, or process disclosed, or represents that its use would not infringe privately owned rights. Reference herein to any specific commercial product, process, or service by its trade name, trademark, manufacturer, or otherwise, does not necessarily constitute or imply its endorsement, recommendation, or favoring by the United States Government or any agency thereof, or the Regents of the University of California. The views and opinions of authors expressed herein do not necessarily state or reflect those of the United States Government or any agency thereof or the Regents of the University of California.

References

- Angéilil, O., Stone, D., Wehner, M., Paciorek, C. J., Krishnan, H., and Collins, W. (2017). An independent assessment of anthropogenic attribution statements for recent extreme temperature and rainfall events. *Journal of Climate*, 30(1):5–16.
- Banerjee, S., Gelfand, A. E., Finley, A. O., and Sang, H. (2008). Gaussian predictive process models for large spatial data sets. *Journal of the Royal Statistical Society: Series B (Statistical Methodology)*, 70(4):825–848.
- Bradley, J. R., Holan, S. H., and Wikle, C. K. (2017). Bayesian hierarchical models with conjugate full-conditional distributions for dependent data from the natural exponential family. *arXiv preprint arXiv:1701.07506*.
- Calder, C. A. (2008). A dynamic process convolution approach to modeling ambient particulate matter concentrations. *Environmetrics*, 19(1):39–48.
- Coles, S. (2001). *An Introduction to Statistical Modeling of Extreme Values*. Lecture Notes in Control and Information Sciences. Springer.
- Damian, D., Sampson, P. D., and Guttorp, P. (2001). Bayesian estimation of semi-parametric non-stationary spatial covariance structures. *Environmetrics*, 12(2):161–178.
- Datta, A., Banerjee, S., Finley, A. O., and Gelfand, A. E. (2016). Hierarchical nearest-neighbor gaussian process models for large geostatistical datasets. *Journal of the American Statistical Association*, 111(514):800–812.
- de Valpine, P., Turek, D., Paciorek, C., Anderson-Bergman, C., Lang, D. T., and Bodik, R. (2017). Programming with models: writing statistical algorithms for general model structures with nimble. *Journal of Computational and Graphical Statistics*, 26:403–413.
- Finley, A. O., Banerjee, S., and Carlin, B. P. (2007). spbayes: an r package for univariate and multivariate hierarchical point-referenced spatial models. *Journal of Statistical Software*, 19(4):1.
- Finley, A. O., Datta, A., Cook, B. C., Morton, D. C., Andersen, H. E., and Banerjee, S. (2018). Efficient algorithms for bayesian nearest-neighbor gaussian processes. *Journal of Computational and Graphical Statistics*, (just-accepted):1–37.

- Fuentes, M. (2001). A high frequency kriging approach for non-stationary environmental processes. *Environmetrics*, 12(5):469–483.
- Fuglstad, G.-A., Lindgren, F., Simpson, D., and Rue, H. (2015). Exploring a new class of non-stationary spatial Gaussian random fields with varying local anisotropy. *Statistica Sinica*, 25:115–133.
- Gramacy, R. B. (2007). tgp: An R package for Bayesian nonstationary, semiparametric nonlinear regression and design by treed Gaussian process models. *Journal of Statistical Software*, 19(9):1–46.
- Guinness, J. (2018). Permutation and grouping methods for sharpening gaussian process approximations. *Technometrics*, (just-accepted).
- Heaton, M. J., Datta, A., Finley, A. O., Furrer, R., Guinness, J., Guhaniyogi, R., Gerber, F., Gramacy, R. B., Hammerling, D., Katzfuss, M., et al. (2018). A case study competition among methods for analyzing large spatial data. *Journal of Agricultural, Biological and Environmental Statistics*, pages 1–28.
- Higdon, D. (1998). A process-convolution approach to modelling temperatures in the North Atlantic Ocean. *Environmental and Ecological Statistics*, 5(2):173–190.
- Higdon, D., Swall, J., and Kern, J. (1999). Non-stationary spatial modeling. *Bayesian Statistics*, 6.
- Hoff, P. and Niu, X. (2012). A covariance regression model. *Statistica Sinica*, 22:729–753.
- Hornik, K. (2012). The comprehensive r archive network. *Wiley Interdisciplinary Reviews: Computational Statistics*, 4(4):394–398.
- Huang, H., Blake, L. R., and Hammerling, D. (2019). Pushing the limit: A hybrid parallel implementation of the multi-resolution approximation for massive data. *arXiv preprint arXiv:1905.00141*.
- Ingebrigtsen, R., Lindgren, F., and Steinsland, I. (2014). Spatial models with explanatory variables in the dependence structure. *Spatial Statistics*, 8(0):20 – 38.
- Kammann, E. and Wand, M. P. (2003). Geoadditive models. *Journal of the Royal Statistical Society: Series C (Applied Statistics)*, 52(1):1–18.
- Katzfuss, M. and Guinness, J. (2017). A general framework for vecchia approximations of gaussian processes. *arXiv preprint arXiv:1708.06302*.
- Katzfuss, M., Guinness, J., and Gong, W. (2018). Vecchia approximations of gaussian-process predictions. *arXiv preprint arXiv:1805.03309*.
- Lauritzen, S. L. (1996). *Graphical models*, volume 17. Clarendon Press.

- Li, Y. and Sun, Y. (2019). Efficient estimation of nonstationary spatial covariance functions with application to high-resolution climate model emulation. *Statistica Sinica*, 29:1209–1231.
- Lindgren, F. and Rue, H. (2015). Bayesian spatial modeling with **R-INLA**. *Journal of Statistical Software*, 63(19):1–25.
- Lindgren, F., Rue, H., and Lindstrom, J. (2011). An explicit link between Gaussian fields and Gaussian Markov random fields: the stochastic partial differential equation approach. *Journal of the Royal Statistical Society: Series B (Statistical Methodology)*, 73(4):423–498.
- Menne, M. J., Durre, I., Korzeniewski, B., McNeal, S., Thomas, K., Yin, X., Anthony, S., Ray, R., Vose, R. S., E. Gleason, B., and Houston, T. G. (2012a). Global Historical Climatology Network - Daily (GHCN-Daily), Version 3. NOAA National Climatic Data Center (accessed 28 January 2019).
- Menne, M. J., Durre, I., Vose, R. S., Gleason, B. E., and Houston, T. G. (2012b). An overview of the Global Historical Climatology Network-Daily database. *Journal of Atmospheric and Oceanic Technology*, 29(7):897–910.
- Neal, R. M. et al. (2003). Slice sampling. *The annals of statistics*, 31(3):705–767.
- Neale, R. B., Chen, C.-C., Gettelman, A., Lauritzen, P. H., Park, S., Williamson, D. L., Conley, A. J., Garcia, R., Kinnison, D., Lamarque, J.-F., Marsh, D., Mills, M., Smith, A. K., Tilmes, S. Vitt, F., Morrison, H., Cameron-Smith, P., Collins, W. D., Iacono, M. J., Easter, R. C., Ghan, S. J., Liu, X., Rasch, P. J., and Taylor, M. A. (2012). Description of the NCAR community atmosphere model (CAM 5.0). Technical report, NCAR Technical Note NCAR/TN-486+STR.
- Nychka, D., Furrer, R., and Sain, S. (2014). *fields: Tools for spatial data*. R package version 7.1.
- Paciorek, C. (2016). *climextRemes: Tools for Analyzing Climate Extremes*. R package version 0.1.2.
- Paciorek, C. J. and Schervish, M. J. (2004). Nonstationary covariance functions for gaussian process regression. In *Advances in neural information processing systems*, pages 273–280.
- Paciorek, C. J. and Schervish, M. J. (2006). Spatial modeling using a new class of nonstationary covariance functions. *Environmetrics*, 17:483–506.
- Reich, B. J., Eidsvik, J., Guindani, M., Nail, A. J., and Schmidt, A. M. (2011). A class of covariate-dependent spatiotemporal covariance functions for the analysis of daily ozone concentration. *The Annals of Applied Statistics*, 5(4):2425–2447.
- Risser, M. and Calder, C. (2017). Local likelihood estimation for covariance functions with spatially-varying parameters: The convoSPAT package for R. *Journal of Statistical Software*, 81(14):1–32.

- Risser, M. D. (2016). Nonstationary spatial modeling, with emphasis on process convolution and covariate-driven approaches. *arXiv preprint arXiv:1610.02447*.
- Risser, M. D. and Calder, C. A. (2015). Regression-based covariance functions for nonstationary spatial modeling. *Environmetrics*, 26(4):284–297.
- Sampson, P. D. and Guttorp, P. (1992). Nonparametric estimation of nonstationary spatial covariance structure. *Journal of the American Statistical Association*, 87(417):108–119.
- Schmidt, A. M., Guttorp, P., and O’Hagan, A. (2011). Considering covariates in the covariance structure of spatial processes. *Environmetrics*, 22(4):487–500.
- Schmidt, A. M. and O’Hagan, A. (2003). Bayesian inference for non-stationary spatial covariance structure via spatial deformations. *Journal of the Royal Statistical Society: Series B (Statistical Methodology)*, 65(3):743–758.
- Stone, D. and Pall, P. (2016). A benchmark estimate of the effect of anthropogenic emissions on the ocean surface. *J. Adv. Model. Earth. Sys.*
- Stone, D. A., Risser, M. D., Angélil, O. M., Wehner, M. F., Cholia, S., Keen, N., Krishnan, H., O’Brien, T. A., and Collins, W. D. (2018). A basis set for exploration of sensitivity to prescribed ocean conditions for estimating human contributions to extreme weather in cam5. 1-1degree. *Weather and climate extremes*, 19:10–19.
- Tibbits, M. M., Groendyke, C., Haran, M., and Liechty, J. C. (2014). Automated factor slice sampling. *Journal of Computational and Graphical Statistics*, 23(2):543–563.
- Vecchia, A. V. (1988). Estimation and model identification for continuous spatial processes. *Journal of the Royal Statistical Society. Series B (Methodological)*, pages 297–312.
- Vianna Neto, J. H., Schmidt, A. M., and Guttorp, P. (2014). Accounting for spatially varying directional effects in spatial covariance structures. *Journal of the Royal Statistical Society: Series C (Applied Statistics)*, 63(1):103–122.

A Matrix calculations for C_y for $d = 2$

For a fixed set of locations $\{\mathbf{s}_1, \dots, \mathbf{s}_n\}$ and conditional on $\boldsymbol{\theta}_y$, we need a fast way to calculate the $n \times n$ matrix $\boldsymbol{\Omega}(\boldsymbol{\theta}_y)$. For now, we keep everything in general terms, i.e., using $\sigma(\cdot)$ and $\boldsymbol{\Sigma}(\cdot)$. In the two-dimensional ($d = 2$) case, the Mahalanobis distance

$$Q(\mathbf{s}, \mathbf{s}') = (\mathbf{s} - \mathbf{s}')^\top \left(\frac{\boldsymbol{\Sigma}(\mathbf{s}) + \boldsymbol{\Sigma}(\mathbf{s}')}{2} \right)^{-1} (\mathbf{s} - \mathbf{s}')$$

can be re-written as follows: using $\mathbf{s} = (s_1, s_2)$, $\mathbf{s}' = (s'_1, s'_2)$ and with

$$\boldsymbol{\Sigma}(\mathbf{s}) = \begin{bmatrix} \Sigma_{11}(\mathbf{s}) & \Sigma_{12}(\mathbf{s}) \\ \Sigma_{12}(\mathbf{s}) & \Sigma_{22}(\mathbf{s}) \end{bmatrix}$$

we can write

$$Q(\mathbf{s}, \mathbf{s}') = a(s_1 - s'_1)^2 + 2b(s_1 - s'_1)(s_2 - s'_2) + c(s_2 - s'_2)^2.$$

Here, a , b , and c are the closed-form elements of $\left(\frac{\Sigma(\mathbf{s}) + \Sigma(\mathbf{s}')}{2}\right)^{-1}$, i.e., writing

$$\frac{\Sigma(\mathbf{s}) + \Sigma(\mathbf{s}')}{2} = \begin{bmatrix} d_{11} & d_{12} \\ d_{12} & d_{22} \end{bmatrix},$$

then

$$a = \frac{d_{22}}{d_{11}d_{22} - d_{12}^2}, \quad b = \frac{-d_{12}}{d_{11}d_{22} - d_{12}^2}, \quad c = \frac{d_{11}}{d_{11}d_{22} - d_{12}^2}.$$

Of course, all of the above values depend on \mathbf{s} and \mathbf{s}' . To calculate the entire distance matrix, i.e., $Q(\mathbf{s}, \mathbf{s}')$ for all pairs of stations, we can convert the above calculation to involve only matrix operations. For the following, we write everything using R syntax.

First, we need matrices of $(s_1 - s'_1)^2$, $(s_1 - s'_1)(s_2 - s'_2)$, and $(s_2 - s'_2)^2$ for all pairs of stations. Define `coords` to be a $n \times 2$ matrix of the coordinates $\{\mathbf{s}_1, \dots, \mathbf{s}_n\}$. The squared univariate distances are easily calculated using `dist()`, but we need to be careful about the the sign of the cross-distance matrix. The following code will calculate these distances correctly:

```
# Univariate distances
dists1 <- as.matrix(dist(coords[,1], upper = T, diag = T))
dists2 <- as.matrix(dist(coords[,2], upper = T, diag = T))

# Adjustment for the sign of the cross-distances
temp1 <- matrix(coords[,1], nrow = n, ncol = n)
temp2 <- matrix(coords[,2], nrow = n, ncol = n)

sgn_mat1 <- ( temp1 - t(temp1) >= 0 )
sgn_mat1[sgn_mat1 == FALSE] <- -1
sgn_mat2 <- ( temp2 - t(temp2) >= 0 )
sgn_mat2[sgn_mat2 == FALSE] <- -1

dist1_sq <- dists1^2
dist2_sq <- dists2^2
dist12 <- sgn_mat1*dists1*sgn_mat2*dists2
```

Note that for a fixed set of coordinates we only need to calculate `dist1_sq`, `dist2_sq`, and `dist12` once, and then pass these around as constants in the **nimble** code.

Next, we can calculate matrix versions of the scaling matrix $\left(\frac{\Sigma(\mathbf{s}) + \Sigma(\mathbf{s}')}{2}\right)^{-1}$. Define `Sigma11` to be a vector $(\Sigma_{11}(\mathbf{s}_1), \dots, \Sigma_{11}(\mathbf{s}_n))$, and similarly `Sigma22` and `Sigma12`, the distance matrix `Dist.mat` containing $\sqrt{Q(\mathbf{s}, \mathbf{s}')}$ for all pairs of stations can be calculated as follows:


```

# Matrix versions for all pairs
mat11_a <- matrix(Sigma11, nrow = N, ncol = N)
mat22_a <- matrix(Sigma22, nrow = N, ncol = N)
mat12_a <- matrix(Sigma12, nrow = N, ncol = N)
mat11 <- 0.5*(mat11_a + t(mat11_a))
mat22 <- 0.5*(mat22_a + t(mat22_a))
mat12 <- 0.5*(mat12_a + t(mat12_a))
# Inverse elements
det12 <- mat11*mat22 - mat12^2
inv11 <- mat22/det12      # above, this is denoted a
inv12 <- -mat12/det12     # above, this is denoted b
inv22 <- mat11/det12     # above, this is denoted c
# Combine with distances
Dist.mat <- sqrt( inv11*dist1_sq + 2*inv12*dist12 + inv22*dist2_sq )

```

The matrix `Dist.mat` can then be fed into the Matérn correlation function.

The second component of the covariance function calculation involves the scaling terms $|\Sigma(\mathbf{s})|^{1/4} |\Sigma(\mathbf{s}')|^{1/4} / \left| \frac{\Sigma(\mathbf{s}) + \Sigma(\mathbf{s}')}{2} \right|^{1/2}$. Again, this can be done using matrix calculations and the same notation as above (using `det12` as calculated before), yielding the matrix `Scale.mat`:

```

det1 <- Sigma11*Sigma22 - Sigma12^2
diag_det1 <- diag(sqrt(sqrt(det1)))
Scale.mat <- diag_det1 %*% sqrt(1/det12) %*% diag_det1

```

Finally, defining `sigma_vec` to be the vector $(\sigma(\mathbf{s}_1), \dots, \sigma(\mathbf{s}_n))$ and `M()` to be a the Matérn correlation function, the full covariance matrix $\Omega(\boldsymbol{\theta}_y)$ is calculated as:

```

Unsc1.corr <- M(Dist.mat, nu)
NS.corr <- Scale.mat*Unsc1.corr
Omega <- diag(sigma_vec) %*% NS.corr %*% diag(sigma_vec)

```

Note that no loops are necessary for these calculations.

B Hyperparameters and required constants for each model

The three likelihood methods and their required constants are provided in Table B.1. The various hyperparameters, prior distributions, and required constants for the process submodels (and prediction) are as follows: Table B.2 contains information for the nugget variance process $\tau(\cdot)$; Table B.3 contains information for the spatial variance process $\sigma(\cdot)$; Tables B.4, B.5, B.6, B.7, and B.8 contain information for the matrix-valued anisotropy process $\Sigma(\cdot)$; and Table B.9 contains information for the mean process $\mu(\cdot)$. Finally, Table B.10 contains the defaults for all of the hyperparameters.

Table B.1: Required constants for each likelihood option.

likelihood = "fullGP"		
Constants	coords	$N \times d$ matrix of coordinate locations
	nu	Scalar; Matérn smoothness parameter (fixed). Defaults to 0.5
likelihood = "NNGP" or likelihood = "SGV"		
Constants	coords	$N \times d$ matrix of coordinate locations
	k	Scalar; number of nearest neighbors to condition upon
	nu	Scalar; Matérn smoothness parameter (fixed). Defaults to 0.5

Table B.2: Sampled hyperparameters, their default priors, and required prior constants for the nugget standard deviation process $\tau(\cdot)$.

<code>tau_model = "constant"</code>		
Parameter	<code>delta</code> (scalar)	Spatially-constant nugget variance: $\log \tau(\mathbf{s}) \equiv \log \sqrt{\delta}$
Prior	Uniform	Lower bound set to 0; upper bound set to <code>tau_HP1</code>
Constants	<code>tau_HP1</code>	Scalar; prior upper bound
Prediction constants	None	

<code>tau_model = "logLinReg"</code>		
Parameter	<code>delta</code>	Vector of log-linear regression coefficients (length p_τ) for the nugget variance, i.e., $\log \tau(\mathbf{s}) = \mathbf{X}_\tau(\mathbf{s})\boldsymbol{\delta}$
Prior	Normal	Each $\delta_i \sim N(0, \text{tau_HP1}^2)$
Constants	<code>tau_HP1</code> <code>X_tau</code> <code>maxAbsLogSD</code>	Scalar; prior st. dev. Design matrix (with p_τ columns); first column should be all ones if intercept is needed Bound on the absolute value of $\log \tau(\mathbf{s})$; necessitated by the fact that proposals for the δ_i combined with certain design matrices can result in numerically non-singular covariance matrices
Prediction constants	<code>PX_tau</code>	Design matrix (with p_τ columns) for the prediction locations; first column should be all ones if intercept is needed

<code>tau_model = "approxGP"</code>		
Parameter	<code>w_tau</code> <code>tauGP_mu</code> <code>tauGP_phi</code> <code>tauGP_sigma</code>	Vector of basis function weights for the knot locations GP mean (scalar) for <code>w_tau</code> GP range (scalar) for <code>w_tau</code> GP standard deviation (scalar) for <code>w_tau</code>
Prior	Gaussian process Normal Uniform Uniform	$\text{tauGP_mu} \sim N(0, \text{tau_HP1}^2)$ Lower bound = 0; upper bound = <code>tau_HP3</code> Lower bound = 0; upper bound = <code>tau_HP4</code>
Constants	<code>tau_knot_coords</code> <code>tau_HP1</code> <code>tau_HP2</code> <code>tau_HP3</code> <code>tau_HP4</code> <code>maxAbsLogSD</code>	Matrix of knot coordinate locations Standard deviation (scalar) for <code>tauGP_mu</code> GP smoothness <code>tauGP_phi</code> upper bound (scalar) <code>tauGP_sigma</code> upper bound (scalar) Bound on the absolute value of $\log \tau(\mathbf{s})$; necessitated by the fact that proposals for <code>w_tau</code> can result in numerically nonsingular covariance matrices
Prediction constants	None	Cross knot/prediction location distances calculated internally.

Table B.3: Sampled hyperparameters, their default priors, and required prior constants for the spatial standard deviation process $\sigma(\cdot)$.

<code>sigma_model = "constant"</code>		
Parameter	<code>alpha</code> (scalar)	Spatially-constant spatial variance: $\log \sigma(\mathbf{s}) \equiv \log \sqrt{\alpha}$
Prior	Uniform	Lower bound set to 0; upper bound set to <code>sigma_HP1</code>
Constants	<code>sigma_HP1</code>	Scalar; prior upper bound
Prediction constants	None	

<code>sigma_model = "logLinReg"</code>		
Parameter	<code>alpha</code>	Vector of log-linear regression coefficients (length p_σ) for the nugget variance, i.e., $\log \sigma(\mathbf{s}) = \mathbf{X}_\sigma(\mathbf{s})\boldsymbol{\alpha}$
Prior	Normal	Each $\delta_i \sim N(0, \text{sigma_HP1}^2)$
Constants	<code>sigma_HP1</code> <code>X_sigma</code> <code>maxAbsLogSD</code>	Scalar; prior st. dev. Design matrix (with p_σ columns); first column should be all ones if intercept is needed Bound on the absolute value of $\log \sigma(\mathbf{s})$; necessitated by the fact that proposals for the α_i combined with certain design matrices can result in numerically non-singular covariance matrices
Prediction constants	<code>PX_sigma</code>	Design matrix (with p_σ columns) for the prediction locations; first column should be all ones if intercept is needed

<code>sigma_model = "approxGP"</code>		
Parameter	<code>w_sigma</code> <code>sigmaGP_mu</code> <code>sigmaGP_phi</code> <code>sigmaGP_sigma</code>	Vector of basis function weights for the knot locations GP mean (scalar) for <code>w_sigma</code> GP range (scalar) for <code>w_sigma</code> GP standard deviation (scalar) for <code>w_sigma</code>
Prior	Gaussian process Normal Uniform Uniform	 <code>sigmaGP_mu</code> $\sim N(0, \text{sigma_HP1}^2)$ Lower bound = 0; upper bound = <code>sigma_HP3</code> Lower bound = 0; upper bound = <code>sigma_HP4</code>
Constants	<code>sigma_knot_coords</code> <code>sigma_HP1</code> <code>sigma_HP2</code> <code>sigma_HP3</code> <code>sigma_HP4</code> <code>maxAbsLogSD</code>	Matrix of knot coordinate locations Standard deviation (scalar) for <code>sigmaGP_mu</code> GP smoothness <code>sigmaGP_phi</code> upper bound (scalar) <code>sigmaGP_sigma</code> upper bound (scalar) Bound on the absolute value of $\log \sigma(\mathbf{s})$; necessitated by the fact that proposals for <code>w_sigma</code> can result in numerically nonsingular covariance matrices
Prediction constants	None	Cross knot/prediction location distances calculated internally.

Table B.4: Sampled hyperparameters, their default priors, and required prior constants for the matrix-valued anisotropy process $\Sigma(\cdot)$.

Sigma_model = "constant"		
Parameter	Sigma_coef1 Sigma_coef2 Sigma_coef3	Spatially-constant anisotropy eigenvalue 1 Spatially-constant anisotropy eigenvalue 2 Spatially-constant rotation parameter
Prior	Uniform Uniform Uniform	Lower bound set to 0; upper bound set to Sigma_HP1 Lower bound set to 0; upper bound set to Sigma_HP1 Lower bound set to 0; upper bound set to $\pi/2$ (for identifiability)
Constants	Sigma_HP1	Scalar; upper bound of the uniform priors for the eigenvalues
Prediction constants	None	

Sigma_model = "constantIso"		
Parameter	Sigma_coef1	Spatially-constant multiplier for the diagonal anisotropy process
Prior	Uniform	Lower bound set to 0; upper bound set to Sigma_HP1
Constants	Sigma_HP1	Scalar; upper bound of the uniform priors for the eigenvalue
Prediction constants	None	

Table B.5: Sampled hyperparameters, their default priors, and required prior constants for the matrix-valued anisotropy process $\Sigma(\cdot)$, continued.

Sigma_model = "covReg"		
Parameter	psi11 psi22 rho gamma1 gamma2	The (1,1) element of Ψ The (2,2) element of Ψ The correlation of Ψ (i.e., $\rho = \psi_{12}/\sqrt{\psi_{11}\psi_{22}}$) First row of Γ ; vector of length p_Σ Second row of Γ ; vector of length p_Σ
Prior	Uniform Uniform Uniform Normal Normal	Lower bound set to 0; upper bound set to Sigma_HP2 Lower bound set to 0; upper bound set to Sigma_HP2 Lower bound set to -1; upper bound set to 1 Each $\gamma_i^{(1)} \sim N(0, \text{Sigma_HP1}^2)$ Each $\gamma_i^{(2)} \sim N(0, \text{Sigma_HP1}^2)$
Constants	Sigma_HP1 Sigma_HP2 X_Sigma maxAnisoRange minAnisoDet	Scalar; prior standard deviation Scalar; upper bound for baseline covariance regression parameters Design matrix (with p_Σ columns); first column should be all ones if intercept is needed Upper bound on $\Sigma_{11}(\mathbf{s})$ and $\Sigma_{22}(\mathbf{s})$ Lower bound on the determinant of the anisotropy process $\Sigma(\mathbf{s})$; certain proposals for the covariance regression coefficients can result in numerical singularities
Prediction constants	PX_Sigma	Design matrix (with p_Σ columns) for the prediction locations; first column should be all ones if intercept is needed

Table B.6: Sampled hyperparameters, their default priors, and required prior constants for the matrix-valued anisotropy process $\Sigma(\cdot)$, continued.

Sigma_model = "compReg"		
Parameter	Sigma_coef1	Vector of length p_Σ ; regression coefficients for the log of the first eigenvalue
	Sigma_coef2	Vector of length p_Σ ; regression coefficients for the log of the second eigenvalue
	Sigma_coef3	Vector of length p_Σ ; regression coefficients for the logit of the scaled rotation parameter
Prior	Normal	Each component is $\sim N(0, \text{Sigma_HP1}^2)$
	Normal	Each component is $\sim N(0, \text{Sigma_HP1}^2)$
	Normal	Each component is $\sim N(0, \text{Sigma_HP1}^2)$
Constants	Sigma_HP1	Scalar; prior standard deviation (default Sigma_HP1 = 10)
	X_Sigma	Design matrix (with p_Σ columns); first column should be all ones if intercept is needed
	maxAnisoRange	Upper bound on $\Sigma_{11}(\mathbf{s})$ and $\Sigma_{22}(\mathbf{s})$
	minAnisoDet	Lower bound on the determinant of the anisotropy process $\Sigma(\mathbf{s})$; certain proposals for the component regression coefficients can result in numerical singularities
Prediction constants	PX_Sigma	Design matrix (with p_Σ columns) for the prediction locations; first column should be all ones if intercept is needed

Sigma_model = "compRegIso"		
Parameter	Sigma_coef1	Vector of length p_Σ ; regression coefficients for the log of the multiplier for the diagonal anisotropy process
Prior	Normal	Each component is $\sim N(0, \text{Sigma_HP1}^2)$
Constants	Sigma_HP1	Scalar; prior standard deviation (default Sigma_HP1 = 10)
	X_Sigma	Design matrix (with p_Σ columns); first column should be all ones if intercept is needed
	maxAnisoRange	Upper bound on $\Sigma(\mathbf{s})$
Prediction constants	PX_Sigma	Design matrix (with p_Σ columns) for the prediction locations; first column should be all ones if intercept is needed

Table B.7: Sampled hyperparameters, their default priors, and required prior constants for the matrix-valued anisotropy process $\Sigma(\cdot)$, continued.

Sigma_model = "npApproxGP"		
Parameter	w1_Sigma w2_Sigma w3_Sigma SigmaGP_mu SigmaGP_phi SigmaGP_sigma	Vector of basis function weights for the knot locations (log of first eigenvalue) Vector of basis function weights for the knot locations (log of second eigenvalue) Vector of basis function weights for the knot locations (logit of scaled rotation) GP mean, of length 2: first for w1_Sigma and w2_Sigma; second for w3_Sigma GP range, of length 2: first for w1_Sigma and w2_Sigma; second for w3_Sigma GP standard deviation, of length 2: first for w1_Sigma and w2_Sigma; second for w3_Sigma
Prior	Gaussian process Gaussian process Gaussian process Normal Uniform Uniform	 Each component $\sim N(0, \text{Sigma_HP1}[i]^2)$ Lower bounds = 0; upper bounds = Sigma_HP3[i] Lower bounds = 0; upper bounds = Sigma_HP4[i]
Constants	Sigma_knot_coords Sigma_HP1 Sigma_HP2 Sigma_HP3 Sigma_HP4 maxAnisoRange minAnisoDet	Matrix of knot coordinate locations 2-vector; SigmaGP_mu standard deviation (for eigenvalue processes and rotation process, respectively) 2-vector; GP smoothness 2-vector; SigmaGP_phi upper bound 2-vector; SigmaGP_sigma upper bound Upper bound on $\Sigma_{11}(\mathbf{s})$ and $\Sigma_{22}(\mathbf{s})$ Lower bound on the determinant of the anisotropy process $\Sigma(\mathbf{s})$; certain proposals for the component regression coefficients can result in numerical singularities
Prediction constants	None	Cross knot/prediction location distances calculated internally.

Table B.8: Sampled hyperparameters, their default priors, and required prior constants for the matrix-valued anisotropy process $\Sigma(\cdot)$, continued.

Sigma_model = "npApproxGPiso"		
Parameter	w1_Sigma SigmaGP_mu SigmaGP_phi SigmaGP_sigma	Vector of basis function weights for the knot locations (log of scalar multiplier) Scalar GP mean for w1_Sigma Scalar GP range for w1_Sigma Scalar GP standard deviation for w1_Sigma
Prior	Gaussian process Normal Uniform Uniform	$\sim N(0, \text{Sigma_HP1}^2)$ Lower bound = 0; upper bound = Sigma_HP3 Lower bound = 0; upper bound = Sigma_HP4
Constants	Sigma_knot_coords Sigma_HP1 Sigma_HP2 Sigma_HP3 Sigma_HP4 maxAnisoRange	Matrix of knot coordinate locations Scalar; SigmaGP_mu standard deviation (for eigen-value processes and rotation process, respectively) Scalar; GP smoothness Scalar; SigmaGP_phi upper bound Scalar; SigmaGP_sigma upper bound Upper bound on $\Sigma(\mathbf{s})$
Prediction constants	None	Cross knot/prediction location distances calculated internally.

Table B.9: Sampled hyperparameters, their default priors, and required prior constants for the mean process $\mu(\cdot)$.

mu_model = "constant"		
Parameter	beta (scalar)	Spatially-constant mean: $\mu(\mathbf{s}) \equiv \beta$
Prior	Normal	$\beta \sim N(0, \text{mu_HP1}^2)$
Constants	mu_HP1	Scalar; prior standard deviation
Prediction constants	None	

mu_model = "linReg"		
Parameter	beta	Vector of linear regression coefficients (length p_μ) for the mean, i.e., $\mu(\mathbf{s}) = \mathbf{X}_\mu(\mathbf{s})\boldsymbol{\beta}$
Prior	Normal	Each $\beta_i \sim N(0, \text{mu_HP1}^2)$
Constants	mu_HP1 X_mu	Scalar; prior standard deviation Design matrix (with p_μ columns); first column should be all ones if intercept is needed
Prediction constants	PX_mu	Design matrix (with p_μ columns) for the prediction locations; first column should be all ones if intercept is needed

mu_model = "zero"		
Parameter	None	The mean is fixed at $\mu(\mathbf{s}) \equiv 0$ for all \mathbf{s}
Prior	n/a	
Constants	n/a	
Prediction constants	None	

Table B.10: Default values for the various hyperparameters. In the table, **maxDist** represents the largest interpoint Euclidean distance for the spatial coordinates of interest. Note: each of the **Sigma_HP** hyperparameters is a vector of length two, with each value fixed at the default listed.

Hyperparameter	Default	Short description
mu_HP1	100	Mean process prior standard deviation
tau_HP1	100	Nugget variance st. dev. or upper bound
tau_HP2	5	Approximate GP smoothness
tau_HP3	maxDist	Upper bound for approximate GP range
tau_HP4	100	Upper bound for approximate GP st. dev.
sigma_HP1	100	Spatial variance st. dev. or upper bound
sigma_HP2	5	Approximate GP smoothness
sigma_HP3	maxDist	Upper bound for approximate GP range
sigma_HP4	100	Upper bound for approximate GP st. dev.
Sigma_HP1	10	St. dev. or upper bound for components of $\Sigma(\mathbf{s})$
Sigma_HP2	10	Upper bound for covReg ψ_{11} and ψ_{22} parameters OR approximate GP smoothness
Sigma_HP3	maxDist	Upper bound for approximate GP ranges
Sigma_HP4	100	Upper bound for approximate GP st. devs.
maxAbsLogSD	10	Upper bound for the absolute value of the log standard deviation; i.e., $-\text{maxAbsLogSD} < \log \tau(\mathbf{s}) < \text{maxAbsLogSD}$ (same for $\sigma(\mathbf{s})$). Used to avoid numerical singularities in the covariance matrix.
maxAnisoDet	1e-5	Lower bound for the determinant of the 2-dimensional anisotropy process (i.e., $\Sigma_{11}(\mathbf{s})\Sigma_{22}(\mathbf{s}) - \Sigma_{12}(\mathbf{s})^2$). Used to avoid numerical singularities in the covariance matrix.
minAnisoRange	maxDist	Upper bound for the diagonal elements of the anisotropy process
nu	0.5	Matérn smoothness for the spatial process (default is the exponential correlation)